Guest Editor's Introduction: Homing Missile Guidance and Control

Neil F. Palumbo

Homing missiles have played an increasingly important role in warfare since the end of World War II. In contrast to inertially guided long-range ballistic missiles, homing missiles guide themselves to intercept targets that can maneuver unpredictably, such as enemy aircraft or anti-ship cruise missiles. Intercepting such threats requires an ability to sense the target location in real time and respond rapidly to changes so that a target intercept can occur. Homing guidance, wherein an onboard sensor provides the target data on which guidance decisions are based, is used to accomplish this intercept. Because of the continually improving quality of target information as the missile closes in, homing guidance provides intercept accuracy that is unsurpassed by any other form of missile guidance. This article serves as the introduction to this Technical Digest *issue on homing missile guidance and control. A number of basic concepts related to guided missiles are introduced in this article to provide the foundational concepts for the subsequent articles. Finally, the flight control and homing guidance concepts that are employed in such systems are discussed in the later articles in this issue.*

INTRODUCTION

The guided missile provides military forces with the capability to deliver munitions rapidly and precisely to selected targets at a distance. This capability establishes an effective means to conduct a wide variety of military missions that range from denying the enemy communications or supply routes, to establishing air superiority, to performing anti-ship cruise missile or ballistic missile defense. Because of this flexibility, guided missiles have attained a remarkable level of importance in military applications and, consequently, in research and development programs. Moreover, the ever-evolving capabilities of enemy systems continue to drive guided missile design toward improved precision, rapid maneuver, and high-speed intercept capabilities.

We begin by defining the difference between an unguided rocket and a guided missile. An unguided rocket is a projectile weapon that (usually) is carrying a warhead and is propelled by an onboard rocket engine.

Like the arrow or cannon ball, an unguided rocket has no ability to change its course once it is airborne. Hence, it flies a ballistic trajectory. It also is notoriously inaccurate, being much more susceptible to targeting errors, wind gusts, and/or other disturbances to its flight path. Examples of unguided rockets include the U.S.-made Hydra-70 family of rockets and the Russian Katyusha.

In contrast to unguided rockets, a guided missile is a projectile provided with a means for altering its flight path *after* it leaves the launching device to effect target intercept. It can do this either autonomously or remotely via a human operator or weapon control system. Thus, a guided missile must carry additional components like inertial sensors, targeting sensors, radio receivers, an autopilot, and a guidance computer. The flight path of a guided missile is adjusted by using movable aerodynamic control surfaces, thrust vectoring, side thrusters, or some combination of these methods. These additions substantially improve engagement accuracy and performance robustness compared with unguided weapons. Examples of guided missiles abound and include the U.S. Navy RIM-66, RIM 156, and RIM 161 Standard Missile variants and the U.S. Army MIM-104 Patriot family of antiballistic missiles.

INERTIAL NAVIGATION VERSUS HOMING GUIDANCE

Inertial guidance systems make possible the precision delivery of long-range ballistic missiles for which the target is, for example, a known set of Earth coordinates. However, these systems are not suitable for guiding missiles against unpredictable targets like maneuvering aircraft or anti-ship cruise missiles or against a target whose location is not known precisely when the missile is launched. Intercepting this kind of threat requires an ability to sense the target location in real time and respond rapidly to changes so that a target intercept can occur. Homing guidance, wherein an onboard sensor provides the target data on which guidance decisions are based, is used to accomplish this intercept. Moreover, because of the continually improving quality of target information as the missile closes in, homing guidance provides intercept accuracy that is unsurpassed by any other form of missile guidance.

In this issue, the focus is squarely on guided missiles that make use of an onboard target sensor and, more specifically, on the related flight control and homing guidance concepts employed in such systems.

HOMING MISSILE TARGET SENSORS

The seeker carried on board a homing missile is categorized as one of the following three general types: passive, semi-active, or active. Figure 1 conceptually illustrates the three types of homing missile seekers.

Common examples of passive systems are infrared (IR) and radio-frequency (RF) seekers. IR seekers detect and track the natural heat signature emanating from a target, whereas passive RF seekers detect stray, or otherwise reflected, RF energy from the target. Passive seekers measure the angular direction of the target relative to the missile, but they do not readily provide range-to-target or closing velocity (range-rate) information,

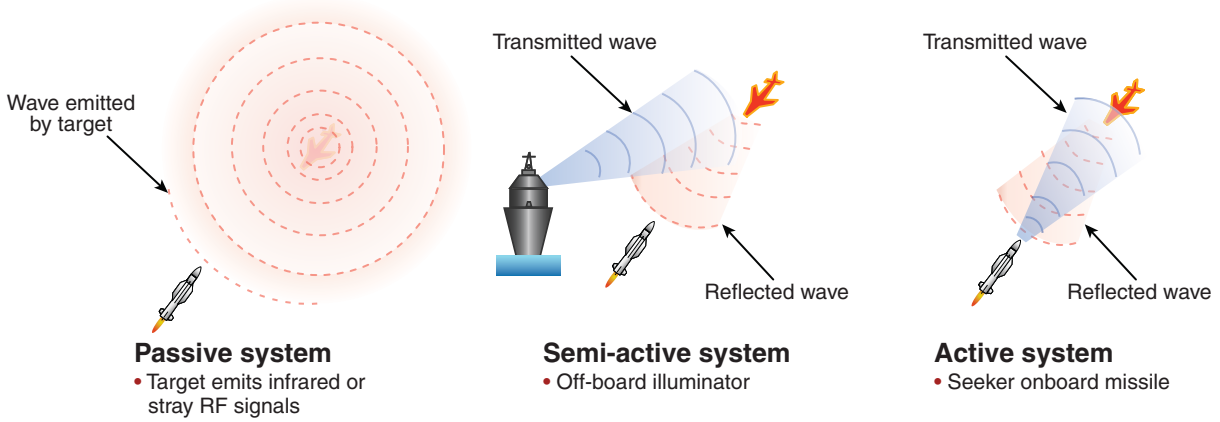

Figure 1. Three basic types of missile seeker systems. A passive seeker does not illuminate the target but, instead, receives energy that emanates from it. Because they do not emit energy, passive seekers make it impossible for the target to determine whether it is being tracked. Semi-active guidance systems illuminate, or designate, the target by directing a beam of light, laser, IR, or RF energy at it. The illuminating beam is transmitted from the launch platform or from an adjacent location. Hence, the illuminating source is largely responsible for target selection in a semi-active system. The passive seeker in the missile then tracks the target using the energy reflected from it. In active seeker guidance systems, an illuminator (transmitter) is added to the missile. Hence, an active guidance system can self-illuminate the target. The addition of an illuminator is costly and adds weight to the missile. However, the missile then is self-sufficient and autonomous after it has locked onto the target.

which is a potential disadvantage in that some guidance techniques require target range and/or range-rate information in addition to azimuth and elevation angles. In these cases, other means of obtaining this information must be employed.

Depending on modality and implementation, semi-active RF seeker systems can provide missile-target closing velocity (range rate) in addition to angular direction of the target. This additional information can help to improve overall guidance accuracy in some instances. Another advantage of semi-active homing is that significantly increased power can be brought to bear on the target without adding to the size and weight of the missile.

Active seeker systems, depending on modality and implementation, can provide missile-target range and range rate in addition to the angular direction of the target. As above, this additional information can be brought to bear in order to improve overall guidance capability. However, power and weight considerations usually restrict active homing to use during the terminal phase of guidance after some other form of guidance has brought the missile to within a short distance of the target.

GUIDED MISSILE PHASES OF FLIGHT

Some guided missiles (usually shorter-range missiles) employ *home-all-the-way* guidance techniques. In these systems, the missile usually sits on a trainable rail launcher (or within a launch canister) that is swiveled to point in a desired direction for launch. The missile must acquire the target (using its own seeker) prior to launch such that, when fired, it can immediately initiate target homing. A variation of this approach is one in which a pre-launch prediction of where the target will be at some post-launch time is provided to the missile. Then, the missile is launched without first acquiring the target organically, and a short inertial boost phase follows. During the inertial boost phase, the missile adjusts its flight path such that it is heading toward the pre-launch prediction of target position. Shortly thereafter, the missile acquires the target using the pre-launch prediction of where to look and initiates target homing.

In the more general case, guided missile flight is partitioned into three phases: boost, midcourse, and terminal guidance phases. Not all guided missiles make use of all three phases.[1,2] However, all precision guided missiles have a terminal phase. Missiles that employ two or more guidance phases are said to execute *multiple-mode* guidance. Figure 2 conceptually illustrates the phases of flight for a multi-mode guided missile.

The need for boost and/or midcourse guidance phases is a function of several factors, including the range at which target intercept will occur (relative to the launch platform) and the types of onboard and off-board sensors available to support the engagement (e.g., off-board radar illuminator and onboard semi-active radar seeker).

During the terminal phase of flight, the guided missile must have a high degree of accuracy and a quick reaction capability. Moreover, near the very end of the terminal phase (often referred to as the endgame), the missile may well be required to maneuver to maximum capability in order to converge on and hit a fast-moving, evasive target. For missile systems that employ a fuze and blast-fragmentation warhead (Standard Missile-2 and Patriot PAC-2 variants are examples of missiles that use a blast-fragmentation warhead), the final miss distance must be less than the warhead's lethal radius. In these systems, the warhead's lethal radius accommodates some lack of guidance precision. On the other hand, a direct-hit missile (Standard Missile-3 and Patriot PAC-3 variants are examples of hit-to-kill missiles) can tolerate only very small "misses" relative to a selected aimpoint on the target body before compromising lethality.

In this issue of the *Technical Digest*, the focus is primarily restricted to guidance techniques related to the terminal phase of flight; however, many of the guidance and control (G&C) concepts that are discussed in the subsequent articles are directly applicable, or can be extended, to the other phases of flight.

FUNCTIONS OF A MISSILE G&C SYSTEM

Many functions must be carried out successfully to intercept and negate the target. Once target detection occurs, a target track must be established by using a tracking sensor, and a decision must be made regarding engageability. If the target is deemed a threat and engageable by the weapon control system, a launch solution is computed, and the missile is launched and boosted to flight speed. Once the missile is launched, the missile G&C system takes over. It must maintain stable flight and converge on the target such that the final distance between the missile and target (the miss distance) is minimized. As mentioned previously, although the missile attempts to minimize the final miss distance, there still can be an appreciable separation between the target payload and interceptor at the closest point of approach. Consequently, a fuzing system and a fragmentation warhead are used to destroy the target. Recent designs for exoatmospheric ballistic missile defense have eliminated the fuze and warhead altogether and rely on body-to-body contact at high closing velocity to achieve a kill. These generally are known as *direct-hit* or *hit-to-kill* systems. In addition to minimizing final miss distance, the missile direction of approach to the target is controlled to provide favorable body-to-body impact or to accommodate fuzing and warhead detonation and to maximize warhead fragments on target. This control of the direction of approach is a key component to

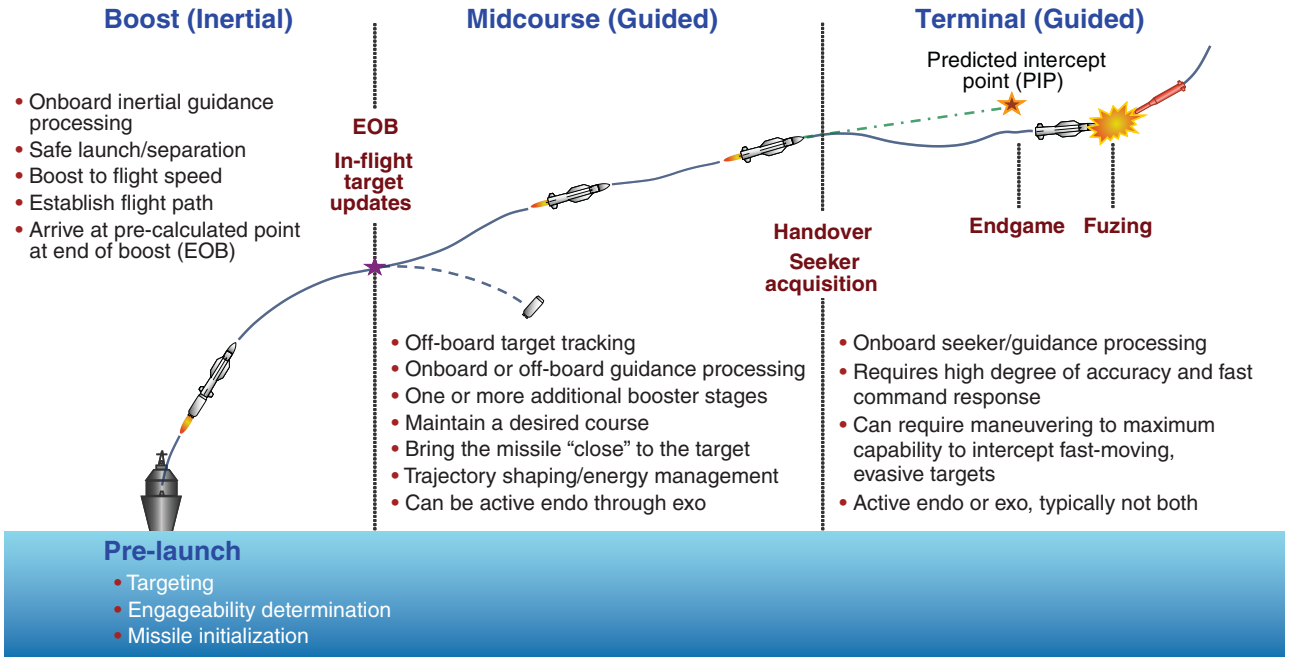
Boost (Inertial)
Midcourse (Guided)
Terminal (Guided)
• Onboard inertial guidance processing
• Safe launch/separation
• Boost to flight speed
• Establish flight path
• Arrive at pre-calculated point at end of boost (EOB)
EOB
In-flight target updates
Predicted intercept point (PIP)
Handover
Seeker acquisition
Endgame
Fuzing
• Off-board target tracking
• Onboard or off-board guidance processing
• One or more additional booster stages
• Maintain a desired course
• Bring the missile "close" to the target
• Trajectory shaping/energy management
• Can be active endo through exo
• Onboard seeker/guidance processing
• Requires high degree of accuracy and fast command response
• Can require maneuvering to maximum capability to intercept fast-moving, evasive targets
• Active endo or exo, typically not both
Pre-launch
• Targeting
• Engageability determination
• Missile initialization

Figure 2. Phases of flight for a multi-mode guided missile. The weapon control system first decides whether the target is engageable. If so, a launch solution is computed, and the missile is initialized, launched, and boosted to flight speed. Inertial guidance typically is employed during the boost phase of flight. Here, the missile is boosted to flight speed and roughly establishes a flight path to intercept the target. Midcourse guidance is an intermediate flight phase whereby the missile receives information from an external source to accommodate guidance to the target. During midcourse, the missile must guide to come within some reasonable proximity of the target and must provide desirable relative geometry against a target when seeker lock-on is achieved (just prior to terminal homing). The terminal phase is the last and, generally, the most critical phase of flight. Depending on the missile capability and the mission, the terminal phase can begin anywhere from tens of seconds down to a few seconds before intercept. The purpose of the terminal phase is to remove the residual errors accumulated during the prior phases and, ultimately, to reduce the final distance between the interceptor and target below some specified level.

maximizing the probability of kill. For homing missiles, pointing to allow seeker acquisition and tracking also is critical. Another important function is to manage interceptor energy to maximize intercept range and maximize missile maneuverability during terminal homing. From this brief discussion, it becomes clear that the missile guidance, navigation, and control (GNC) system must perform a variety of complex functions to enable a successful target intercept.

GNC SYSTEM FUNCTIONAL ARCHITECTURE

The aggregate capability of the guided missile subsystems (inertial measurement unit, target seeker, propulsion, etc.) will define the maximum performance potential of the weapon. It is the role of the missile GNC system to functionally integrate these subsystems to ensure that all requirements are met and that lethality is maximized against the targets of interest. GNC system operation is based on the principle of feedback. Moreover, all fielded guided missile GNC systems are particular examples of the feedback concept in Fig. 3, which illustrates the traditional GNC paradigm that employs a decoupled architecture composed of guidance filter, guidance law, autopilot, and inertial navigation subsystems.

As indicated in Fig. 3, the traditional architecture separates guidance and flight control functions. The inertial navigation system (INS) provides the position, velocity, acceleration, angular orientation, and angular velocity of the vehicle by measuring the inertial linear acceleration and inertial angular velocity applied to the system. The information from the INS is used throughout missile flight to support guidance and flight control functions. The guidance filter receives noisy target measurement data from the homing sensor and estimates the relevant target states, the selection of which are design-dependent.[3–5] For example, a Cartesian guidance filter can provide estimates of target position, velocity, and acceleration with respect to a Cartesian reference frame. Equivalently, relative (target–missile) position, relative velocity, and target acceleration can be estimated. Typically, a linear or extended Kalman filter is used.[3,6–8] The guidance law takes the instantaneous target-state estimates as input and determines what the interceptor direction of travel should be to intercept the

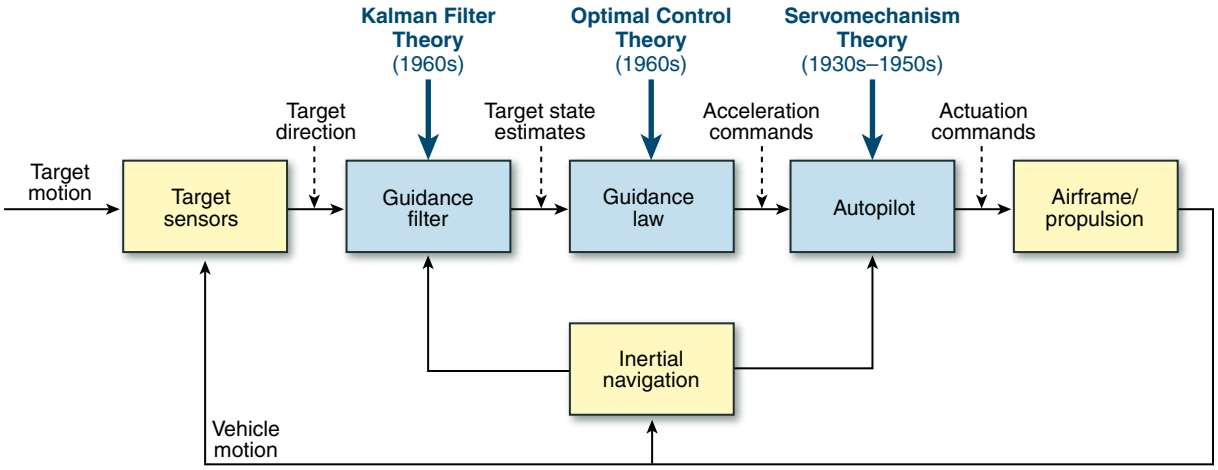

Figure 3. Traditional missile GNC topology. The traditional GNC topology for a guided missile comprises guidance filter, guidance law, autopilot, and inertial navigation components. Each component may be synthesized by using a variety of techniques, the most popular of which are indicated here in blue text.

target. It typically is an anticipatory function in that it generates guidance commands to put the missile on a collision course with the target. One of the oldest and most frequently used guidance laws is proportional navigation (PN).[1,9,10] PN generates guidance commands proportional to the line-of-sight rate between the guided missile and target. (In this issue, the article "Basic Principles of Homing Guidance" discusses PN in some detail. Then, a more comprehensive treatment of modern missile guidance laws and associated synthesis techniques is presented in the article "Modern Homing Missile Guidance Theory and Techniques.") Finally, the autopilot is responsible for stabilization and command following.[1,11–15] The autopilot receives the guidance commands and issues the relevant aerodynamic (e.g., fin), thrust-vector, or divert control commands necessary to achieve the commanded acceleration.

In a decoupled G&C paradigm such as that illustrated in Fig. 3, it is typical to design each component separately and, as suggested by the figure, a variety of synthesis techniques may be adopted for each component design (some dominant techniques are indicated in Fig. 3). Moreover, when designing the guidance filter and guidance law, it is typical to make simplifying assumptions regarding missile response to acceleration commands. These facts can lead to an overly conservative or suboptimal design. In addition, once the individual components are designed, it is typical for the system as a whole to be iteratively tuned, adjusted, and/or modified until satisfactory performance is achieved.

Recent research has led to prototype G&C architectures that consider integration of the guidance and flight control systems. Moreover, modern synthesis techniques are applied to achieve a design that optimally integrates the missile subsystems, thereby leading to a consistently high probability of kill across the threat space.[4,16–20] Figure 4 illustrates a notional integrated G&C (IGC) architecture[12,21–26] and emphasizes the notion that G&C component separation has less meaning in an IGC design.

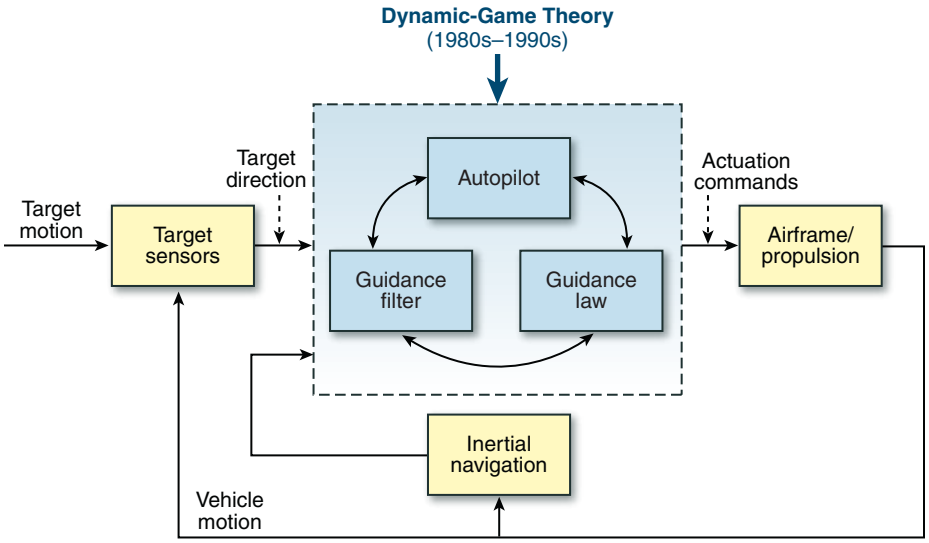

Figure 4. IGC topology. In an IGC system, there is no separation of the guidance and flight control functions.

OUTLINE OF THE ISSUE

This article has discussed a number of basic concepts related to homing missile GNC meant to provide context focus for this issue. In summary, I have defined the difference between guided and unguided weapons, distinguished inertial guidance versus homing guidance, characterized multi-mode guidance, and introduced the feedback structure for missile GNC.

The rest of the articles in this issue of the *Digest* provide more in-depth discussions related to the general concepts introduced here. Referring back to Fig. 3, we see that the flight control function on the right is a key component to achieving the overall mission in that it takes the guidance commands and translates them to achieve the called-for missile maneuvers. This topic alone is quite complex, and a comprehensive treatment of it is far beyond the limited scope of this issue. Thus, the article "Overview of Missile Flight Control Systems" is just as the title implies: it presents a general overview of flight control.

The subsequent three articles address the core focus of this issue, that is, homing missile (terminal) guidance. The article "Basic Principles of Homing Guidance" provides a conceptual foundation with respect to homing guidance. In this article, a basic geometric and notational framework is established, the PN guidance concept is developed from the ground up, line-of-sight reconstruction (the collection and orchestration of the various inertial and target sensor measurements necessary to support homing guidance) is introduced, and many of the challenges associated with designing effective homing guidance systems (noise sources, radome errors, etc.) are discussed.

PN was *the* guidance law of choice (for practical implementation and performance reasons) through the 1970s and beyond. Even today, many guided missiles still employ PN or a close variant. However, by the mid-1970s, it became clear that the types of threats (highly maneuverable aircraft, supersonic cruise missiles, tactical and strategic ballistic missile reentry vehicles, etc.) that were emerging could render PN-guided weapons less effective. That realization, in conjunction with the advancing state of the art in computer miniaturization and computational power, led to a flood of new ideas and synthesis techniques for homing guidance. The preeminent technique centered on linear-quadratic optimization methods. The article "Modern Homing Missile Guidance Theory and Techniques" is a fundamental treatment of guidance laws from this perspective. Here, PN is rederived from the linear-quadratic perspective, and a number of new guidance laws are discussed, compared, and contrasted.

Regardless of the specific structure of the guidance law (e.g., PN versus some other variant), it typically is assumed during the design stage that all of the states necessary to mechanize the implementation are (directly) available for feedback and uncorrupted by noise. In reality, this is not possible; the available measurements require filtering to mitigate noise effects and, oftentimes, other unmeasured states must be derived (estimated) to accommodate guidance law mechanization. Hence, guidance filters take raw sensor data as inputs and derive (estimate) and filter the signals upon which the guidance law operates. The article "Guidance Filter Fundamentals" discusses this topic, and guidance filtering methods are introduced with an emphasis on the discrete-time Kalman filter.

Six-degree-of-freedom simulations are effective tools for cost and risk reduction during the development and deployment of missile systems. The article "Six-Degree-of-Freedom Digital Simulations for Missile Guidance, Navigation, and Control" presents a brief historical review of missile simulations and their practical uses. The authors then examine the requirements of a digital simulation independent of the models and outline current simulation designs. They also characterize the essential models found in a missile GNC simulation and discuss the different levels of detail (fidelity) for these models, while also considering some practical engineering questions that the simulation may help answer based on the level of model fidelity.

G&C algorithms are diverse in type and complexity. However, they all have adjustable parameters that affect their operation and, consequently, guided missile performance. The "tuning" process, whereby optimum values for the adjustable parameters are determined, is a critical challenge in algorithm design. Analytical techniques often are unavailable, and manual "analyze-and-iterate" methods can be time-consuming (and suboptimal). The article "Tuning Missile Guidance and Control Algorithms Using Simultaneous Perturbation Stochastic Approximation" discusses an automated, simulation-based approach to G&C algorithm optimization. Some practical challenges of G&C algorithm tuning, as well as effective solutions to these challenges, also are discussed.

CONCLUSION

For more than 65 years, APL has been making critical contributions to the defense of our naval forces. Within the context of air and missile defense, it is expected that these challenges will continue to mount as threat aircraft and missile systems evolve and become more sophisticated. These evolving challenges, in turn, will continue to drive future guided missile interceptor designs and the associated performance requirements. The articles in this issue should provide the reader with an appreciation for the basic technical and design challenges associated with the missile G&C problem as it is applied to missile interceptor design.

REFERENCES

[1]Locke, A. S., *Principles of Guided Missile Design*, D. Van Nostrand, New York (1955).

[2]Witte, R. W., and McDonald, R. L., "Standard Missile: Guidance System Development," *Johns Hopkins APL Tech. Dig.* **2**(4), 289–298 (1981).

[3]Bar-Shalom, Y., Li, X. R., and Kirubarajan, T., *Estimation with Applications to Tracking and Navigation*, John Wiley and Sons, New York (2001).

[4]Ben-Asher, J. Z., and Yaesh, I., *Advances in Missile Guidance Theory*, American Institute of Aeronautics and Astronautics, Reston, VA (1998).

[5]Zarchan, P., *Tactical and Strategic Missile Guidance*, 4th Ed., American Institute of Aeronautics and Astronautics, Reston, VA (1997).

[6]Brown, R. G., and Hwang, P. Y. C., *Introduction to Random Signals and Applied Kalman Filtering*, 2nd Ed., John Wiley and Sons, New York (1992).

[7]Chui, C. K., and Chen, G., *Kalman Filtering with Real-Time Applications*, 3rd Ed., Springer, New York (1999).

[8]Zarchan, P., and Musoff, H., *Fundamentals of Kalman Filtering: A Practical Approach*, American Institute of Aeronautics and Astronautics, Reston, VA (2000).

[9]Pue, A. J., *Proportional Navigation and an Optimal-Aim Guidance Technique*, JHU/APL Memorandum F1C(2)-80-U-024 (7 May 1980).

[10]Shneydor, N. A., *Missile Guidance and Pursuit: Kinematics, Dynamics and Control*, Horwood Publishing, London (1998).

[11]Etkin, B., *Dynamics of Atmospheric Flight*, John Wiley and Sons, New York (1972).

[12]Jackson, P. B., *TOMAHAWK 1090 Autopilot Improvements: Pitch-Yaw-Roll Autopilot Design*, JHU/APL Memorandum F1E(90)U-1-305 (1 Aug 1990).

[13]O'Connell, J., "Stability of the Epic Autopilot," RCA Internal Report ND-E-MIS-T-2151 (26 Oct 1982).

[14]Rugh, W. J., and Shamma, J. S., "Research on Gain Scheduling," *Automatica* **36**(10), 1401–1425 (2000).

[15]Jackson, P. B., *Multivariable Control System Design Method for Independent Assessment of Block IVA Autopilot*, JHU/APL Memorandum A1E(99)U-3-057 (20 May 1999).

[16]Basar, T., and Bernhard, P., *H-Infinity Optimal Control and Related Minimax Design Problems*, Birkhäuser, Boston (1995).

[17]Cloutier, J. R., D'Souza, N., and Mracek, C. P., "Nonlinear Regulation and Nonlinear H-Infinity Control Via the State-Dependent Riccati Equation Technique: Parts 1 and 2," *First Int. Conf. on Nonlinear Problems in Aviation and Aerospace*, pp. 117–141 (9–11 May 1996).

[18]Hammett, K. D., "Control of Nonlinear Systems via State Feedback State-Dependent Riccati Equation Techniques," Ph.D. dissertation, Air Force Institute of Technology (June 1997).

[19]Rhee, I., and Speyer, J. L., "A Game Theoretic Approach to a Finite-Time Disturbance Attenuation Problem," *IEEE Trans. Autom. Control* **36**(9), 1021–1032 (Sep 1991).

[20]Cloutier, J. R., Mracek, C. P., Ridgely, D. B., and Hammett, K. D., "State Dependent Riccati Equation Techniques: Theory and Applications," *American Control Conf.*, Albuquerque, NM, Workshop Tutorial No. 6 (1998).

[21]Lin, C. F., Wang, Q., Speyer, J. L., Evers, J. H., and Cloutier, J. R., "Integrated Estimation, Guidance, and Control System Design Using Game Theoretic Approach," *Proc. American Control Conf.*, Chicago, IL, pp. 3220–3224 (1992).

[22]Palumbo, N. F., *A Fully Integrated Guidance and Control System for the Highly Responsive Missile Control System—Advanced Technology Demonstration: Preliminary Development and Results*, JHU/APL Memorandum A1E(96)U-5-196 (7 Oct 1996).

[23]Palumbo, N. F., *A Fully Integrated Guidance and Control System Based on the Disturbance Attenuation Design Approach*, JHU/APL Memorandum A1E(98)U-5-5 (12 Jan 1998).

[24]Palumbo, N. F., and Jackson, T. D., "Integrated Missile Guidance and Control: A State-Dependent Riccati Differential Equation Approach," in *Proc. 1999 IEEE Int. Conf. on Control Applications*, Kohala Coast, HI, pp. 243–248 (22–27 Aug 1999).

[25]Lin, C. F., Ohlmeyer, E., Bibel, J. E., and Malyevac, S., "Optimal Design of Integrated Missile Guidance and Control," *1998 World Aviation Conf.*, Anaheim, CA, No. AIAA-985519 (28–30 Sep 1998).

[26]Palumbo, N. F., and Casper, S. G., "Integration of a Missile Autopilot, Guidance Filter and Guidance Law," *AIAA/BMDO Technology Conf.*, San Diego, CA (Jul 2000).

The Author

Neil F. Palumbo

Neil F. Palumbo is a member of APL's Principal Professional Staff and is the Group Supervisor of the Guidance, Navigation, and Control Group within the Air and Missile Defense Department. He joined APL in 1993 after having received a Ph.D. in electrical engineering from Temple University that same year. His interests include control and estimation theory, fault-tolerant restructurable control systems, and neuro-fuzzy inference systems. Dr. Palumbo also is a lecturer for the JHU Whiting School's Engineering for Professionals program. He is a member of the Institute of Electrical and Electronics Engineers and the American Institute of Aeronautics and Astronautics. His email address is neil.palumbo@jhuapl.edu.

The *Johns Hopkins APL Technical Digest* can be accessed electronically at **www.jhuapl.edu/techdigest**.

Basic Principles of Homing Guidance

Neil F. Palumbo, Ross A. Blauwkamp, and Justin M. Lloyd

This article provides a conceptual foundation with respect to homing guidance upon which the next several articles are anchored. To this end, a basic geometric and notational framework is first established. Then, the well-known and often-used proportional navigation guidance concept is developed. The mechanization of proportional navigation in guided missiles depends on several factors, including the types of inertial and target sensors available on board the missile. Within this context, the line-of-sight reconstruction process (the collection and orchestration of the inertial and target sensor measurements necessary to support homing guidance) is discussed. Also, guided missiles typically have no direct control over longitudinal acceleration, and they maneuver in the direction specified by the guidance law by producing acceleration normal to the missile body. Therefore, we discuss a guidance command preservation technique that addresses this lack of control. The key challenges associated with designing effective homing guidance systems are discussed, followed by a cursory discussion of midcourse guidance for completeness' sake.

INTRODUCTION

The key objective of this article is to provide a broad conceptual foundation with respect to homing guidance but with sufficient depth to adequately support the articles that follow. During guidance analysis, it is typical to assume that the missile is on a near-collision course with the target. The implications of this and other assumptions are discussed in the first section, *Handover Analysis*. The next section, *Engagement Kinematics*, establishes a geometric foundation for analysis that is used in the subsequent sections of this and the other guidance-related articles in this issue. In particular, a line-of-sight (LOS) coordinate frame is introduced upon which the kinematic equations of motion are developed; this coordinate frame supports the subsequent derivation of

proportional navigation (PN) guidance. Over the past 50 years, PN has proven both reliable and robust, thereby contributing to its continued use. The *Development of PN Guidance Law* section presents the derivation of and discusses this popular and much-used technique. The subsequent section, *Mechanization of PN*, discusses how PN may be implemented in a homing missile. Key drivers here are the type of sensor that is used to detect and track the target, how the sensor is mounted to the missile, and how the LOS (rate) measurement is developed. The next section, *Radome/Irdome Design Requirements*, briefly discusses the functional requirements imposed on modern missile radomes. This is followed by an expanded section on *Guidance System Design Challenges*. Here, the contributors to the degradation of guidance system performance (radome error and others) are discussed. Then, *Guidance Command Preservation* presents a technique for commanding acceleration commands perpendicular to the missile body that will effectively maneuver the missile in the desired guidance direction. Although this article is mainly concerned with terminal homing concepts, the *Midcourse Guidance* section briefly discusses issues and requirements associated with the midcourse phase of flight.

Handover Analysis

When terminal guidance concepts are being developed or related systems analysis is being performed, it typically is assumed that the missile interceptor is on a collision course (or nearly so) with the target. In reality, this is not usually the case. For example, there can be significant uncertainty in target localization, particularly early in the engagement process, that precludes satisfaction of a collision course condition prior to terminal homing. Moreover, the unpredictable nature of future target maneuvers (e.g., target booster staging events, energy management steering, coning of a ballistic missile reentry vehicle, or the weaving or spiraling maneuvers of an anti-ship cruise missile) can complicate the development of targeting, launch, and/or (midcourse) guidance solutions that guarantee collision course conditions before initiation of terminal homing. In addition, cumulative errors are associated with missile navigation and the effects of unmodeled missile dynamics that all add together to complicate satisfaction of a collision course condition. For simplicity, all of these errors can be collectively regarded as uncertainties in the location of the target with respect to the missile interceptor. Thus, if the interceptor is launched (and subsequently guided during midcourse) on the basis of estimated (predicted) future target position, then, at the time of acquisition by the onboard seeker, the actual target position will be displaced from its predicted position. Figure 1 notionally illustrates this condition, where $\bar{\mathbf{r}}$ is the LOS vector between the missile and the predicted target location; $\bar{\mathbf{1}}_{\mathbf{r}_{LOS}} = \bar{\mathbf{r}}/\|\bar{\mathbf{r}}\|$ is the unit vector along the LOS; $\bar{\mathbf{v}}_T$ and $\bar{\mathbf{v}}_M$ are the velocity vectors of the target and missile, respectively; $\bar{\mathbf{v}}_R = \bar{\mathbf{v}}_T - \bar{\mathbf{v}}_M$ is the relative velocity vector; and $\bar{\mathbf{e}}$ is the displacement error between predicted and true target position.

As discussed, ideally, the relative velocity vector is along the LOS to the true future target position (at the time of intercept). However, Fig. 1 depicts a more realistic condition where the relative velocity is along the LOS to the estimated future target position in space. For this case, the interceptor will miss the target unless it applies corrective maneuvers.

Figure 1 illustrates that the displacement error, $\bar{\mathbf{e}}$, can be decomposed into two components: one along ($\bar{\mathbf{e}}_{\|}$) and one perpendicular ($\bar{\mathbf{e}}_{\perp}$) to the predicted target LOS. This decomposition is expressed in Eq. 1:

$$\begin{aligned} \bar{\mathbf{e}}_{\|} &= (\bar{\mathbf{e}} \bullet \bar{\mathbf{1}}_{\mathbf{r}_{LOS}})\,\bar{\mathbf{1}}_{\mathbf{r}_{LOS}} \\ \bar{\mathbf{e}}_{\perp} &= \bar{\mathbf{1}}_{\mathbf{r}_{LOS}} \times (\bar{\mathbf{e}} \times \bar{\mathbf{1}}_{\mathbf{r}_{LOS}}) . \end{aligned} \tag{1}$$

In this equation, $\bar{\mathbf{x}} \bullet \bar{\mathbf{y}}$ represents the dot (scalar) product between the two vectors $\bar{\mathbf{x}}$ and $\bar{\mathbf{y}}$, and $\bar{\mathbf{x}} \times \bar{\mathbf{y}}$ represents the cross (vector) product between the two vectors. Note that, because the relative velocity vector, $\bar{\mathbf{v}}$, is along the LOS to the predicted target location, the error $\bar{\mathbf{e}}_{\|}$ will alter the time of intercept but does not contribute to the final miss distance. Consequently, the miss distance that must be removed by the interceptor after transition to terminal homing is contained in $\bar{\mathbf{e}}_{\perp}$ (i.e., target uncertainty normal to the LOS).

Homing missile guidance strategies (guidance laws) dictate the manner in which the missile will guide to intercept, or rendezvous with, the target. The feedback nature of homing guidance allows the guided missile (or, more generally, "the pursuer") to tolerate some

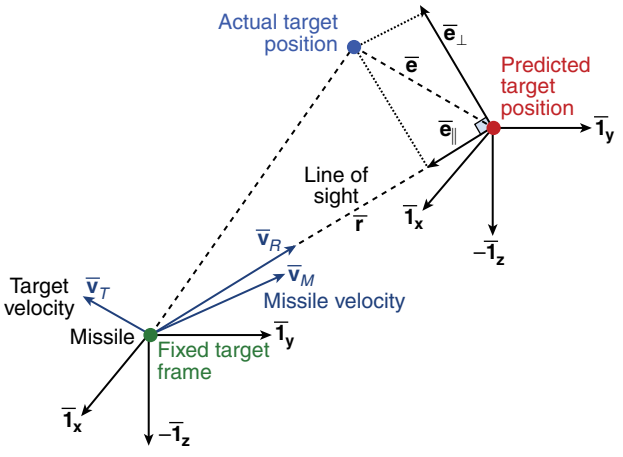

Figure 1. To assist in simplifying the analysis of handover to terminal homing, all of the contributing navigation and engagement modeling errors are collectively regarded as uncertainties to the location of the target with respect to the missile at handover.

level of (sensor) measurement uncertainties, errors in the assumptions used to model the engagement (e.g., unanticipated target maneuver), and errors in modeling missile capability (e.g., deviation of actual missile speed of response to guidance commands from the design assumptions). Nevertheless, the selection of a guidance strategy and its subsequent mechanization are crucial design factors that can have substantial impact on guided missile performance. Key drivers to guidance law design include the type of targeting sensor to be used (passive IR, active or semi-active RF, etc.), accuracy of the targeting and inertial measurement unit (IMU) sensors, missile maneuverability, and, finally yet important, the types of targets to be engaged and their associated maneuverability levels. We will begin by developing a basic model of the engagement kinematics. This will lay the foundation upon which PN, one of the oldest and most common homing missile guidance strategies, is introduced.

Engagement Kinematics: The Line-of-Sight Coordinate System

The development presented here follows the one given in Ref. 1. In the sequel, the following notation is used: $\mathbf{X} = n \times m$ (read n-by-m) matrix of scalar elements $x_{i,j}$, $i = 1 \ldots n$, $j = 1 \ldots m$; $\bar{\mathbf{x}} = n \times 1$ vector of scalar elements x_i, $i = 1 \ldots n$; $\|\bar{\mathbf{x}}\| = \sqrt{\sum_{i=1}^{n} x_i^2}$ = Euclidean vector norm of $\bar{\mathbf{x}}$; $\bar{\mathbf{1}}_{\mathbf{x}} = \bar{\mathbf{x}}/\|\bar{\mathbf{x}}\| = n \times 1$ unit vector (e.g., $\|\bar{\mathbf{1}}_{\mathbf{x}}\| = 1$) in the direction of $\bar{\mathbf{x}}$; $\delta/\delta t$ = time derivative with respect to a fixed (inertial) coordinate system; and d/dt = time derivative with respect to a rotating coordinate system.

Consider the engagement geometry shown in Fig. 2, where $\bar{\mathbf{r}}_M$ and $\bar{\mathbf{r}}_T$ are the position vectors of the missile interceptor and target with respect to a fixed coordinate frame of reference (represented by the triad $\{\bar{\mathbf{1}}_{\mathbf{x}}, \bar{\mathbf{1}}_{\mathbf{y}}, \bar{\mathbf{1}}_{\mathbf{z}}\}$). Consequently, we define the relative position vector of the target with respect to the missile as shown in Eq. 2:

$$\bar{\mathbf{r}} = \bar{\mathbf{r}}_T - \bar{\mathbf{r}}_M . \tag{2}$$

The relative position vector can be written as $\bar{\mathbf{r}} = R\bar{\mathbf{1}}_{\mathbf{r}}$, where $R = \|\bar{\mathbf{r}}\|$ is the target–missile range, and $\bar{\mathbf{1}}_{\mathbf{r}}$ is the unit vector directed along $\bar{\mathbf{r}}$ (we refer to $\bar{\mathbf{1}}_{\mathbf{r}}$ as the LOS unit vector). Differentiating the relative position vector, $\bar{\mathbf{r}} = R\bar{\mathbf{1}}_{\mathbf{r}}$, with respect to the fixed coordinate system, we obtain the following expression for relative velocity $\bar{\mathbf{v}}$:

$$\bar{\mathbf{v}} \equiv \frac{\delta}{\delta t}\bar{\mathbf{r}} = \dot{R}\bar{\mathbf{1}}_{\mathbf{r}} + R\frac{\delta}{\delta t}\bar{\mathbf{1}}_{\mathbf{r}} . \tag{3}$$

From Eq. 3, one can see that the rate of change of the relative position vector (i.e., relative velocity) comprises two components: (*i*) a change in $\bar{\mathbf{r}}$ as a result of a change in length ($\dot{R}$) and (*ii*) a change in direction (a rotation) as a result of the rate of change of the LOS unit vector.

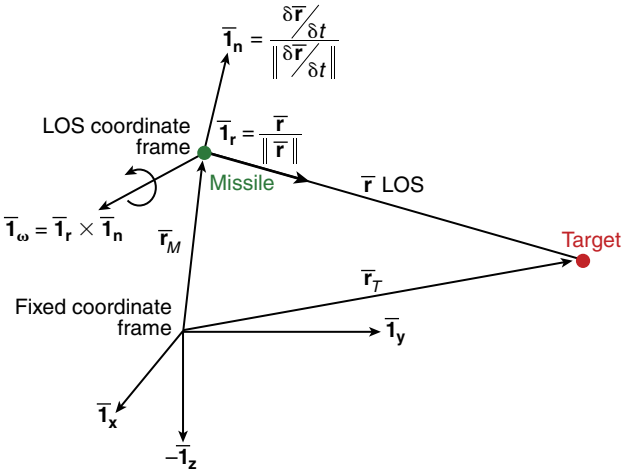

Figure 2. In the LOS coordinate frame, the LOS rate is perpendicular to the LOS direction and rotation of the LOS takes place about the $\bar{\mathbf{1}}_{\boldsymbol{\omega}}$.

We define this change in direction by the vector $\bar{\mathbf{n}}$ as given in Eq. 4:

$$\bar{\mathbf{n}} \equiv \frac{\delta}{\delta t}\bar{\mathbf{1}}_{\mathbf{r}} . \tag{4}$$

Consequently, a second unit vector, $\bar{\mathbf{1}}_{\mathbf{n}}$, is defined to be in the direction of $\bar{\mathbf{n}}$ as shown:

$$\bar{\mathbf{1}}_{\mathbf{n}} = \frac{\delta\bar{\mathbf{1}}_{\mathbf{r}}/\delta t}{\|\delta\bar{\mathbf{1}}_{\mathbf{r}}/\delta t\|} = \frac{\bar{\mathbf{n}}}{\|\bar{\mathbf{n}}\|} . \tag{5}$$

Finally, to complete the definition of the (right-handed) LOS coordinate system, a third unit vector, $\bar{\mathbf{1}}_{\boldsymbol{\omega}}$, is defined as the cross product of the first two:

$$\bar{\mathbf{1}}_{\boldsymbol{\omega}} = \bar{\mathbf{1}}_{\mathbf{r}} \times \bar{\mathbf{1}}_{\mathbf{n}} . \tag{6}$$

In general, the angular velocity of the LOS coordinate system with respect to an inertial reference frame is given by $\dot{\bar{\varphi}} = \dot{\phi}_{\mathbf{r}}\bar{\mathbf{1}}_{\mathbf{r}} + \dot{\phi}_{\mathbf{n}}\bar{\mathbf{1}}_{\mathbf{n}} + \dot{\phi}_{\boldsymbol{\omega}}\bar{\mathbf{1}}_{\boldsymbol{\omega}}$, where the components of the angular velocity are given in Eq. 7:

$$\begin{aligned} \dot{\phi}_{\mathbf{r}} &= \dot{\bar{\varphi}} \cdot \bar{\mathbf{1}}_{\mathbf{r}} \\ \dot{\phi}_{\mathbf{n}} &= \dot{\bar{\varphi}} \cdot \bar{\mathbf{1}}_{\mathbf{n}} \\ \dot{\phi}_{\boldsymbol{\omega}} &= \dot{\bar{\varphi}} \cdot \bar{\mathbf{1}}_{\boldsymbol{\omega}} . \end{aligned} \tag{7}$$

Thus, upon reexamination of Eq. 4, we note that the LOS rate, $\bar{\mathbf{n}}$, can be expressed as shown in Eq. 8:

$$\bar{\mathbf{n}} = \frac{d}{dt}\bar{\mathbf{1}}_{\mathbf{r}} + \dot{\bar{\varphi}} \times \bar{\mathbf{1}}_{\mathbf{r}} . \tag{8}$$

On the right-hand side of Eq. 8, the expression $d\bar{\mathbf{1}}_{\mathbf{r}}/dt$ represents the time derivative of the LOS unit vector with respect to a rotating coordinate frame, and $\dot{\bar{\varphi}}$ is

the angular velocity of the rotating frame with respect to the inertial frame. The former component is equal to zero (i.e., the LOS unit vector is a constant). Therefore, the LOS rate and corresponding unit vectors simplify to the following expressions:

$$\begin{aligned}\bar{\mathbf{n}} &= \dot{\bar{\varphi}} \times \bar{\mathbf{1}}_{\mathbf{r}} \\ \bar{\mathbf{1}}_{\mathbf{n}} &= \frac{\dot{\bar{\varphi}} \times \bar{\mathbf{1}}_{\mathbf{r}}}{\| \dot{\bar{\varphi}} \times \bar{\mathbf{1}}_{\mathbf{r}} \|} .\end{aligned} \tag{9}$$

Thus, from Eq. 3, the relative velocity expression is given as

$$\bar{\mathbf{v}} = \dot{R}\bar{\mathbf{1}}_{\mathbf{r}} + R(\dot{\bar{\varphi}} \times \bar{\mathbf{1}}_{\mathbf{r}}) . \tag{10}$$

The typical guided missile control variable is interceptor acceleration. Thus, taking the derivative of Eq. 10, and using Eq. 9, we obtain an expression for the relative acceleration:

$$\begin{aligned}\frac{\delta}{\delta t}\bar{\mathbf{v}} &= \ddot{R}\bar{\mathbf{1}}_{\mathbf{r}} + \dot{R}\frac{\delta}{\delta t}\bar{\mathbf{1}}_{\mathbf{r}} + \dot{R}(\dot{\bar{\varphi}} \times \bar{\mathbf{1}}_{\mathbf{r}}) + R(\ddot{\bar{\varphi}} \times \bar{\mathbf{1}}_{\mathbf{r}}) + R\left(\dot{\bar{\varphi}} \times \frac{\delta}{\delta t}\bar{\mathbf{1}}_{\mathbf{r}}\right) \\ &= \ddot{R}\bar{\mathbf{1}}_{\mathbf{r}} + 2\dot{R}(\dot{\bar{\varphi}} \times \bar{\mathbf{1}}_{\mathbf{r}}) + R(\ddot{\bar{\varphi}} \times \bar{\mathbf{1}}_{\mathbf{r}}) + R[\dot{\bar{\varphi}} \times (\dot{\bar{\varphi}} \times \bar{\mathbf{1}}_{\mathbf{r}})] .\end{aligned} \tag{11}$$

Next, using the definition of $\dot{\bar{\varphi}}$ in Eq. 7 and the fact that $\bar{\mathbf{1}}_{\mathbf{r}} = [1 \quad 0 \quad 0]^T$, we expand the term $\dot{\bar{\varphi}} \times \bar{\mathbf{1}}_{\mathbf{r}} \equiv \bar{\mathbf{n}}$ in Eq. 11, which results in the following relation:

$$\dot{\bar{\varphi}} \times \bar{\mathbf{1}}_{\mathbf{r}} = \det \begin{vmatrix} \bar{\mathbf{1}}_{\mathbf{r}} & \bar{\mathbf{1}}_{\mathbf{n}} & \bar{\mathbf{1}}_{\boldsymbol{\omega}} \\ \dot{\phi}_{\mathbf{r}} & \dot{\phi}_{\mathbf{n}} & \dot{\phi}_{\boldsymbol{\omega}} \\ 1 & 0 & 0 \end{vmatrix} = \dot{\phi}_{\boldsymbol{\omega}}\bar{\mathbf{1}}_{\mathbf{n}} - \dot{\phi}_{\mathbf{n}}\bar{\mathbf{1}}_{\boldsymbol{\omega}} . \tag{12}$$

Here, $\det|\cdot|$ represents taking the determinant of a matrix. From Eq. 4, the direction of $\bar{\mathbf{n}}$ can have no component along $\bar{\mathbf{1}}_{\boldsymbol{\omega}}$. Thus, we conclude $\dot{\phi}_{\mathbf{n}} = 0$ and obtain the result in Eq. 13:

$$\dot{\bar{\varphi}} \times \bar{\mathbf{1}}_{\mathbf{r}} = \dot{\phi}_{\boldsymbol{\omega}}\bar{\mathbf{1}}_{\mathbf{n}} . \tag{13}$$

In Eq. 13, $\dot{\phi}_{\boldsymbol{\omega}} \equiv |\bar{\mathbf{n}}|$. Using Eq. 13, the other cross-product terms in Eq. 11 yield the following results:

$$\begin{aligned}\dot{\bar{\varphi}} \times (\dot{\bar{\varphi}} \times \bar{\mathbf{1}}_{\mathbf{r}}) &= -\dot{\phi}_{\boldsymbol{\omega}}^2\bar{\mathbf{1}}_{\mathbf{r}} + \dot{\phi}_{\mathbf{r}}\dot{\phi}_{\boldsymbol{\omega}}\bar{\mathbf{1}}_{\boldsymbol{\omega}} \\ \ddot{\bar{\varphi}} \times \bar{\mathbf{1}}_{\mathbf{r}} &= \ddot{\phi}_{\boldsymbol{\omega}}\bar{\mathbf{1}}_{\mathbf{n}} .\end{aligned} \tag{14}$$

Using Eqs. 13 and 14 in Eq. 11, we obtain the desired expression for relative acceleration:

$$\begin{aligned}\frac{\delta^2}{\delta t^2}\bar{\mathbf{r}} &= \bar{\mathbf{a}}_T - \bar{\mathbf{a}}_{\mathrm{M}} \\ &= (\ddot{R} - R\dot{\phi}_{\boldsymbol{\omega}}^2)\bar{\mathbf{1}}_{\mathbf{r}} + (2\dot{R}\dot{\phi}_{\boldsymbol{\omega}} + R\ddot{\phi}_{\boldsymbol{\omega}})\bar{\mathbf{1}}_{\mathbf{n}} + (R\dot{\phi}_{\boldsymbol{\omega}}\dot{\phi}_{\mathbf{r}})\bar{\mathbf{1}}_{\boldsymbol{\omega}} .\end{aligned} \tag{15}$$

From Eq. 15, the components of relative acceleration in the LOS coordinate frame can be written as shown in Eq. 16:

$$\begin{aligned}(\bar{\mathbf{a}}_T - \bar{\mathbf{a}}_{\mathrm{M}}) \cdot \bar{\mathbf{1}}_{\mathbf{r}} &= \ddot{R} - R\dot{\phi}_{\boldsymbol{\omega}}^2 \\ (\bar{\mathbf{a}}_T - \bar{\mathbf{a}}_{\mathrm{M}}) \cdot \bar{\mathbf{1}}_{\mathbf{n}} &= 2\dot{R}\dot{\phi}_{\boldsymbol{\omega}} + R\ddot{\phi}_{\boldsymbol{\omega}} \\ (\bar{\mathbf{a}}_T - \bar{\mathbf{a}}_{\mathrm{M}}) \cdot \bar{\mathbf{1}}_{\boldsymbol{\omega}} &= R\dot{\phi}_{\boldsymbol{\omega}}\dot{\phi}_{\mathbf{r}} .\end{aligned} \tag{16}$$

Development of PN Guidance Law

Many guided missiles employ some version of PN as the guidance law during the terminal homing phase. Surface-to-air, air-to-air, and air-to-surface missile engagements, as well as space applications (including rendezvous), use PN in one form or another as a guidance law.[1–7] A major advantage of PN, contributing to its longevity as a favored guidance scheme over the last five decades, is its relative simplicity of implementation. The most basic PN implementations require low levels of information regarding target motion as compared with other more elaborate schemes (some are discussed in the next article in this issue, "Modern Homing Missile Guidance Theory and Techniques"), thus simplifying onboard sensor requirements. Moreover, it has proven to be relatively reliable and robust. As also will be seen in the next article in this issue, under certain conditions and (simplifying) assumptions about target and missile characteristics, the PN law is an optimal guidance strategy in the sense of minimizing the terminal miss distance.

In order to develop the PN guidance strategy, we first look to the components of Eq. 16 for sufficient conditions to achieve an intercept. Looking at the first component, sufficient conditions for an intercept are (*i*) the LOS rate is zero ($\dot{\phi}_{\boldsymbol{\omega}} = 0$), (*ii*) interceptor capability to accelerate along the LOS is greater than or equal to target acceleration along the LOS ($\bar{\mathbf{a}}_{\mathrm{M}} \cdot \bar{\mathbf{1}}_{\mathbf{r}} \geq \bar{\mathbf{a}}_T \cdot \bar{\mathbf{1}}_{\mathbf{r}}$), and (*iii*) the initial range rate along the LOS is negative ($\dot{R}(0) < 0$). In this case, missile-to-target range (R) will decrease linearly ($(\bar{\mathbf{a}}_T - \bar{\mathbf{a}}_{\mathrm{M}}) \cdot \bar{\mathbf{1}}_{\mathbf{r}} = 0$) or quadratically ($(\bar{\mathbf{a}}_T - \bar{\mathbf{a}}_{\mathrm{M}}) \cdot \bar{\mathbf{1}}_{\mathbf{r}} < 0$) with respect to time and, eventually, pass through zero.

From the discussion above, the interceptor must accelerate such as to null the LOS rate ($\dot{\phi}_{\boldsymbol{\omega}}$). We look to the second component of Eq. 16 to determine how this can be done. We first define closing velocity as $V_c \equiv -\dot{R}$. Note that for an approaching trajectory $\dot{R} < 0$; thus $V_c > 0$. If, for the moment, we treat closing velocity and range as constant, then taking the Laplace transform of the second component of Eq. 16 yields the following polynomial in s:

$$(\bar{\mathbf{a}}_T(s) - \bar{\mathbf{a}}_{\mathrm{M}}(s)) \cdot \bar{\mathbf{1}}_{\mathbf{n}} = (sR - 2V_c)\dot{\phi}_{\boldsymbol{\omega}}(s) . \tag{17}$$

In Eq. 17, s represents the Laplace transform variable. Thus, if we define interceptor acceleration perpendicular to the LOS to be $\bar{\mathbf{a}}_{\mathrm{M}}(s) \cdot \bar{\mathbf{1}}_{\mathbf{n}} = \Lambda\dot{\phi}_{\boldsymbol{\omega}}(s)$, then, from Eq. 17, we can write the transfer function from target accelera-

tion (perpendicular to the LOS) to the corresponding LOS rate:

$$\frac{\dot{\phi}_{\boldsymbol{\omega}}(s)}{(\bar{\mathbf{a}}_T(s) \bullet \bar{\mathbf{I}}_{\mathbf{n}})} = \frac{1}{(sR - 2V_c + \Lambda)} . \tag{18}$$

Referring to Eq. 18, to ensure a stable system, we require $\Lambda > 2V_c$. This leads to what is known as the true PN guidance law shown in Eq. 19:

$$\bar{\mathbf{a}}_{\mathrm{M}} \bullet \bar{\mathbf{I}}_{\mathbf{n}} = NV_c\dot{\phi}_{\boldsymbol{\omega}},\ N > 2 . \tag{19}$$

As is clear from the previous development, true PN commands missile acceleration normal to the LOS. This is, perhaps, more obvious by referring back to Eq. 13 and rewriting Eq. 19 as shown in Eq. 20:

$$\bar{\mathbf{a}}_{\mathrm{M}_c} = NV_c\dot{\bar{\varphi}} \times \bar{\mathbf{I}}_{\mathbf{r}},\ N > 2 . \tag{20}$$

Here, $\bar{\mathbf{a}}_{\mathrm{M}_c}$ a represents commanded missile acceleration normal to the LOS. Achieved missile acceleration is physically realized through aerodynamic control surface deflections, control thruster operation, or a combination of both. Thus, Eq. 20 also emphasizes the fact that the development of PN assumes a no-lag missile response (i.e., the missile is assumed to respond instantly to, and achieve perfectly, the guidance command).

We will simply mention another variant of PN, referred to a pure proportional navigation (PPN). The names given to these variants are somewhat arbitrary, but these names have stuck. The general three-dimensional version of PPN can be expressed as shown in Eq. 21.

$$\bar{\mathbf{a}}_{\mathrm{M}_c} = k\dot{\bar{\varphi}} \times \bar{\mathbf{v}}_{\mathrm{M}} . \tag{21}$$

Here, k is the navigation gain. Clearly, PPN commands missile acceleration normal to the missile velocity vector, $\bar{\mathbf{v}}_{\mathrm{M}}$.

In view of the importance of the PN law in missile guidance and space applications, considerable analytical study has been conducted regarding the behavior of a missile guided under PN. Since the differential equations governing PN motion, even when considering kinematics only, are highly nonlinear, only limited success has been achieved in solving these equations analytically.

Mechanization of PN

Here, we discuss how PN can be mechanized in a homing missile. Central to this topic is the type of sensor that is used to detect and track the target: whether it is a passive (e.g., IR), semi-active, or active (e.g., RF or laser) sensor and, as important, how it is mounted to the missile.

As discussed, the conventional implementation of PN requires closing velocity and LOS rate information to produce the guidance (acceleration) commands. If we assume (for clarity) that the engagement is planar, then we can rewrite Eq. 20 as shown below, where $\dot{\lambda}$ is the LOS rate in an inertial frame of reference:

$$a_{\mathrm{M}_c} = NV_c\dot{\lambda} . \tag{22}$$

Thus, implementation of the PN guidance law in three dimensions dictates the necessity to measure LOS rate in two sensor instrument axes that are mutually perpendicular to the sensor boresight (near-coincident with the measured LOS to the target).

As mentioned previously, the way in which closing velocity (V_c) and LOS rate ($\dot{\lambda}$) information is obtained to mechanize PN guidance (Eq. 22) is a function of the type of target sensor that is used and how it is mounted to the missile body. Acquiring closing velocity information depends primarily on the target sensor type. Given an (onboard) active or semi-active RF system, for example, the observed Doppler frequency of the target return can be used to develop a good estimate of closing velocity, V_c. In other implementations, missile-to-target range or closing velocity can be periodically up-linked to the missile to facilitate PN guidance.

The way in which LOS rate ($\dot{\lambda}$) information is derived depends on the type of target sensor that is used and how it is mounted to the missile. For example, a space-stabilized sensor (could be RF, IR, or laser) is mounted on a gimbaled platform to increase the field of regard of the sensor and to isolate it from missile body motion. Conversely, tracking systems that do not require a large field of regard or that employ an IR focal plane array, for example, are fixed to the body (strapdown systems). Here, we will consider space-stabilized systems. Before introducing the details on how to derive LOS rate, we briefly discuss space-stabilized target sensor systems.

Various space-stabilized designs are possible, but a typical design is one in which two mutually perpendicular gimbals are employed along with rate gyros used for platform stabilization and LOS/LOS rate reconstruction. (Typically, these systems rely on the missile autopilot for roll stabilization.) Such gimbaled platforms use a servomotor in each axis to accommodate seeker pointing. Hence, we will define a space-stabilized seeker to be composed of the target sensor (antenna/energy-collecting device and a receiver), gimbals (and associated servomotors), gyros, and the necessary control electronics. The necessary seeker functions are as follows: (*i*) track the target continuously after acquisition, (*ii*) provide a measure of the LOS angle (λ) or LOS angular rate ($\dot{\lambda}$), (*iii*) stabilize the seeker against significant missile body rate motion (pitching and yawing rate) that may be much larger than the LOS rate to be measured,

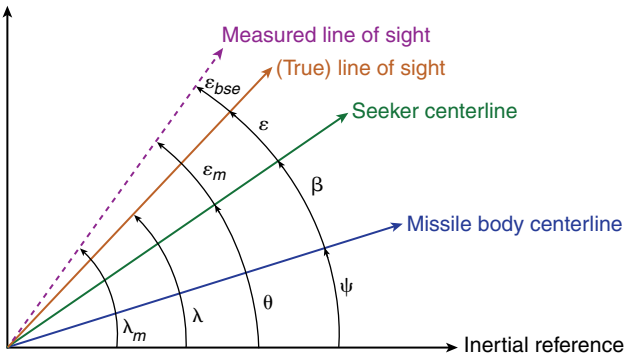

Figure 3. Illustration of the two-dimensional definitions of the various angles often used when analyzing the LOS reconstruction process.

and (*iv*) measure the closing velocity, if possible.[8] Item *iv* is possible to achieve with radar systems but is difficult with IR systems.

Seeker pointing is accomplished by an outer gimbal rotation β_O about the missile body *y* axis (pitch), followed by an inner gimbal rotation β_I about the subsequent *z* axis. These two rotations are used to define the coordinate transformation from the missile body frame (*B*) to the seeker coordinate frame (*S*), as shown in Eq. 23:

$$C_B^S = \begin{bmatrix} \cos\beta_O \cos\beta_I & \sin\beta_I & -\sin\beta_O \cos\beta_I \\ -\cos\beta_O \sin\beta_I & \cos\beta_I & \sin\beta_O \sin\beta_I \\ \sin\beta_O & 0 & \cos\beta_O \end{bmatrix}. \quad (23)$$

In order to outline possible approaches to derive LOS rate for guidance purposes, we will refer to Fig. 3, where we have defined the following angular quantities: ψ is the inertial angle to the missile body centerline; θ is the inertial angle to the seeker centerline (inertial dish angle); β is the gimbal angle (angle between seeker boresight and missile centerline); ε is the true tracking error (epsilon) between the LOS and seeker centerline; ε_{bse} is a perturbation to the true epsilon caused by radome refraction of the RF energy or irdome distortion of IR energy as it passes through the material; ε_m is the measured epsilon; λ is the true inertial LOS angle; and λ_m is the measured, or reconstructed, inertial LOS angle.

Tracking of a target requires the continuous pointing of the sensor beam at the target. As illustrated in Fig. 4, the receiver measures the tracking error (ε_m) with respect to seeker coordinates. (Primary contributors to tracking error are discussed later.) The measured tracking error, in turn, is used by the tracking system (the seeker track loop) to drive the seeker dish angle θ (via servomotor torquing of the gimbals) such as to minimize the tracking error, thereby keeping the target in the field of view. Consequently, the seeker dish rate, $\dot{\theta}$, is approximately equal to the inertial LOS rate. The transfer function of LOS rate to seeker dish rate can be approximated by the following first-order transfer function:

$$\frac{\dot{\theta}}{\dot{\lambda}} = \frac{1}{\tau_s s + 1}. \quad (24)$$

In this relationship, τ_s is the seeker track-loop time constant. Thus, the seeker dish rate will lag the LOS rate. The accuracy to which the seeker is stabilized places fundamental limitations on the homing precision of the missile.

One possible LOS rate estimation scheme is shown in Fig. 5, which illustrates a simplified block diagram comprising the seeker, guidance computer, flight control system, and body rate aerodynamic transfer function. In Fig. 5, the Laplace operator is indicated by *s*. For simplicity, the flight control system (i.e., the combined representation of the control surface actuators, aerodynamics, and autopilot) is expressed as the transfer function represented by $G_{FC}(s)$. The guidance system is represented as a simplified LOS rate guidance filter followed by a PN guidance law. The combined guidance system transfer function is shown in Eq. 25, where τ_f is the guidance filter time constant:

$$\frac{a_c}{\dot{\lambda}_m} = \frac{NV_c}{\tau_f s + 1}. \quad (25)$$

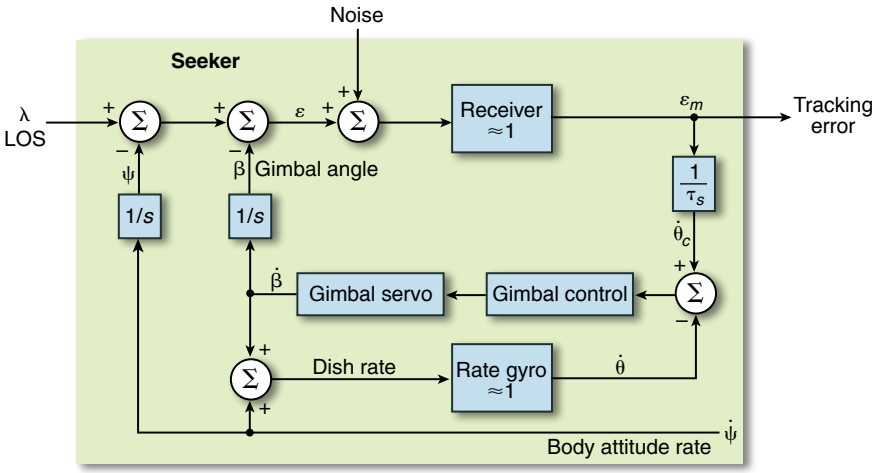

Figure 4. Simplified planar model of a gimbaled seeker track loop (without radome effects). In this configuration, the commanded dish rate is proportional to the tracking error.

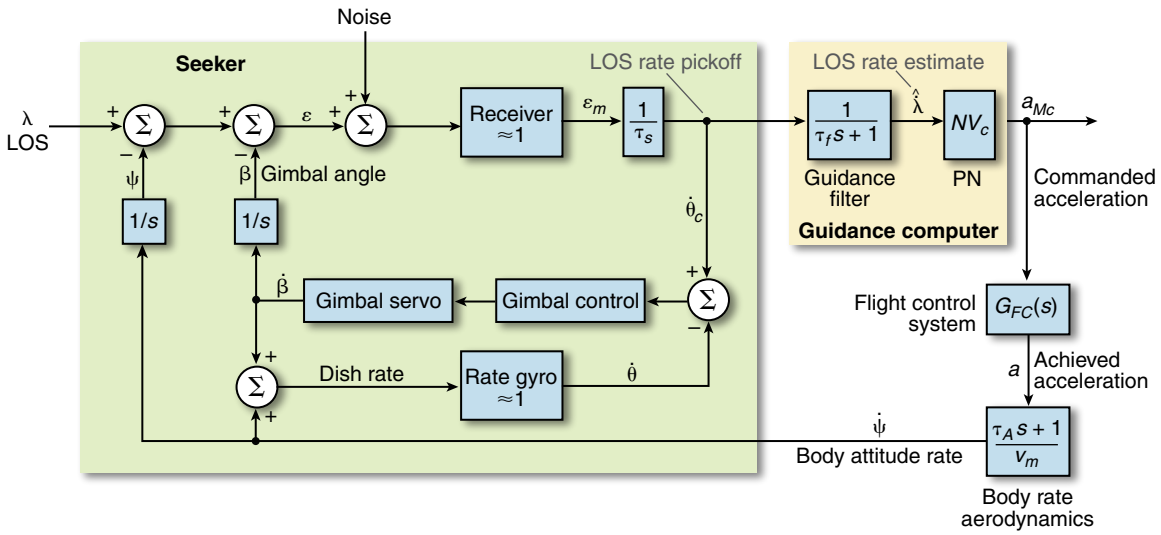

Figure 5. Simplified planar model of a traditional LOS rate reconstruction approach that directly supplies an LOS rate measurement to the guidance computer. Note that the LOS rate pickoff is assumed to be proportional to the boresight error measurement. The measured LOS rate is subsequently filtered to mitigate measurement noise and then applied to the PN homing guidance law.

Moreover, the transfer function from commanded acceleration (from the guidance law) to missile body rate ($\dot{\psi}$) is approximated by the following aerodynamic transfer function, where τ_A is the turning rate time constant and v_m is missile velocity:

$$\frac{\dot{\psi}}{a_c} = \frac{\tau_A s + 1}{v_m} . \tag{26}$$

In this approach, the fact that the LOS rate is embedded in the tracking error (ε_m) is exploited. As illustrated, a LOS rate estimate is derived by appropriately filtering the receiver tracking error scaled by the seeker track-loop time constant.

Other approaches can be used to derive LOS rate for homing guidance purposes; these are generally referred to as either LOS reconstruction or LOS rate reconstruction. We next outline three alternative techniques (two LOS reconstructions and one LOS rate reconstruction).

LOS Reconstruction

As shown in Fig. 3, LOS reconstruction works to construct a measured LOS, λ_m, in an inertial frame of reference. The measured LOS then is filtered (via an appropriate guidance filter) to derive an estimate of LOS rate for guidance purposes. Two different LOS reconstruction approaches are as follows:[9]

1. Integrate the seeker gyro output and sum it with the measured tracking error. A block diagram of this approach is shown in Fig. 6. Mathematically, this approach can be expressed as Eq. 27:

$$\lambda_m = \varepsilon_m + \int \dot{\theta} dt . \tag{27}$$

2. Integrate the output of the missile body rate gyro, obtained from the missile IMU, and sum the integrated IMU gyro output together with the seeker gimbal angle and the measured tracking error. We illustrate this approach in the block diagram shown in Fig. 7. This approach is expressed mathematically as shown in Eq. 28:

$$\lambda_m = \varepsilon_m + \beta + \int \dot{\psi} dt . \tag{28}$$

From Fig. 3, it is clear that the two concepts are algebraically equivalent in the absence of noise and assuming perfect instruments (no gyro biases, drift, etc.); however, in practice, this is not the case. Moreover, we note that, in general, the guidance filters for the two approaches are not necessarily the same (e.g., for the simplified guidance filters shown in the figures, the filter time constants, represented by τ_f, are not necessarily the same). The fundamentals of guidance filtering will be discussed in the companion article in this issue "Guidance Filter Fundamentals." It is shown in Ref. 9 that the two LOS reconstruction approaches can yield significantly different results when noise and imperfect instruments are used. How these differences manifest themselves depends on the quality of the measurements and instruments that are used.

LOS Rate Reconstruction

A guidance signal also can be generated by differentiating the tracking error and adding it to the seeker rate gyro output. For practical purposes, taking the derivative of the tracking error is accom-

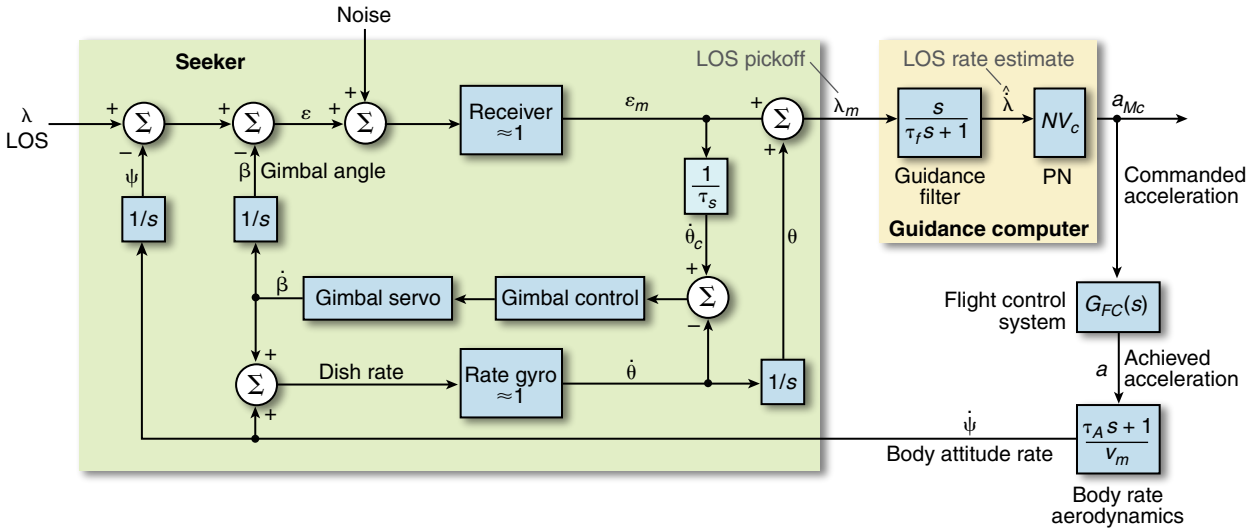

Figure 6. LOS reconstruction approach 1 wherein the seeker gyro output is integrated and summed with the measured tracking error to form an LOS measurement. The measured LOS is subsequently passed to the guidance computer, where it is filtered to extract an LOS rate and then applied to the PN guidance law.

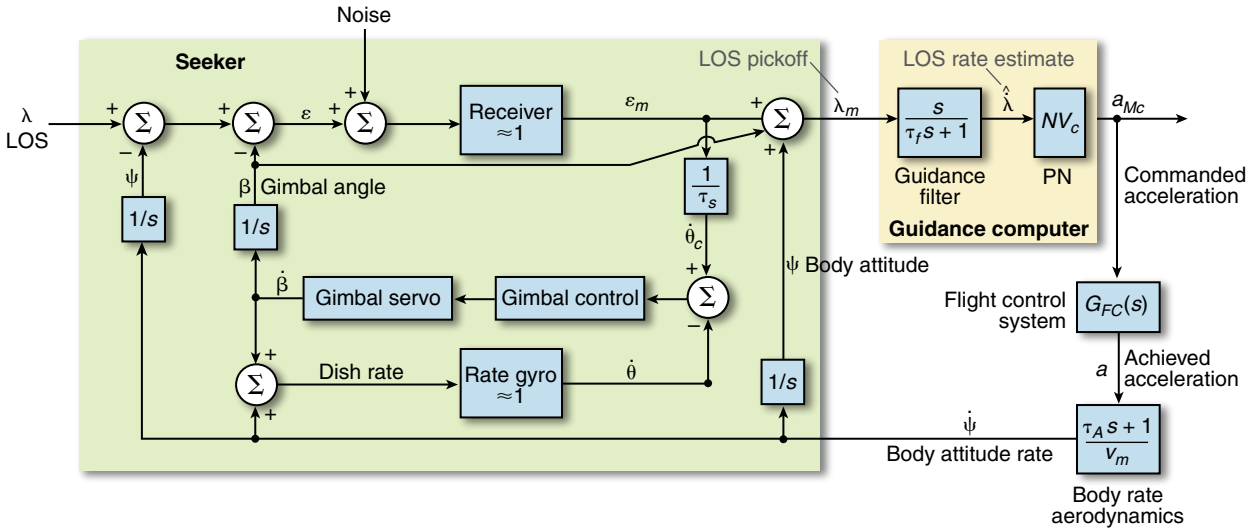

Figure 7. LOS reconstruction approach 2 wherein the output of the missile body rate gyro (via the missile IMU) is integrated and summed together with the seeker gimbal angle and the measured tracking error to develop an LOS measurement. The measured LOS is subsequently passed to the guidance computer, where it is filtered to extract an LOS rate and then applied to the PN guidance law.

plished by using a lead network such as that given below:

$$\frac{s}{\tau_D s + 1}. \tag{29}$$

Figure 8 illustrates this approach. Here, τ_D is the time constant of the lead network. As shown, the reconstructed LOS rate is filtered by an appropriate guidance filter (here represented by a simplified lag filter with time constant τ_f) to derive a LOS rate estimate. This method may lead to excessive amplification of the receiver noise as a result of the differentiation process. However, in Ref. 10, it is shown that LOS rate reconstruction can work well if the missile turning rate (i.e., responsiveness to commands) is very fast.

Radome/Irdome Design Requirements

In endoatmospheric engagements, a radome (or irdome) is required in order to protect the onboard seeker from the elements. For exoatmospheric vehicles, a radome/irdome is not necessarily required. The key dome requirements are summarized below[8]:

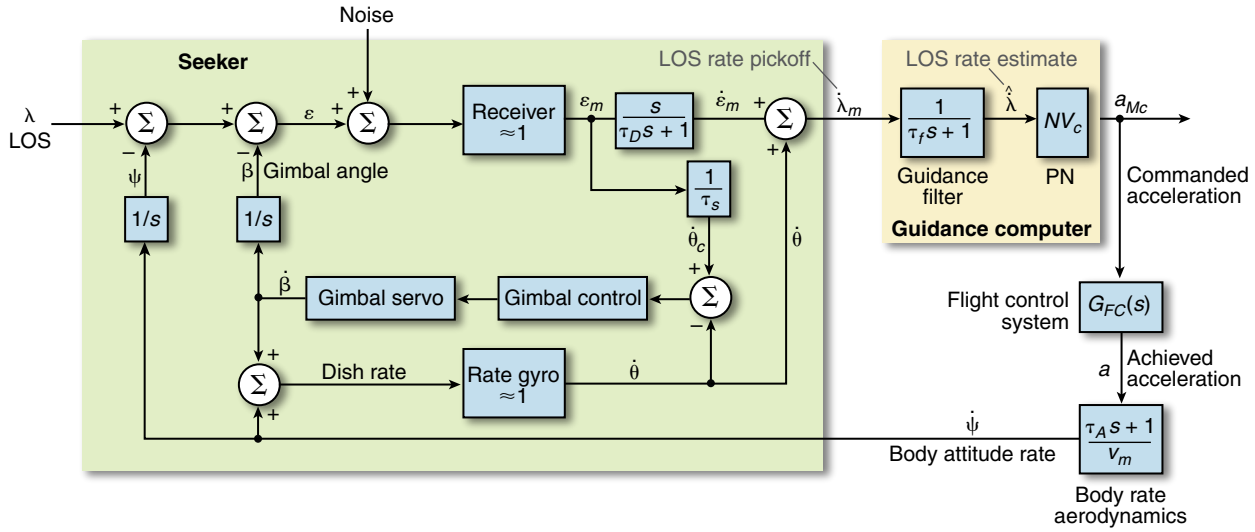

Figure 8. Simplified planar model of an alternate LOS rate reconstruction approach that can directly supply an LOS rate measurement to the guidance computer. Note that the LOS rate reconstruction differences between this figure and Fig. 5. As before, the measured LOS rate is subsequently filtered to mitigate measurement noise and then applied to the PN homing guidance law.

1. It must convey the energy with minimum loss.
2. It must convey the energy with minimum distortion, particularly angular distortion because this creates a parasitic feedback loop that can have a significant negative impact on guidance performance (discussed in more detail below).
3. It must have minimum aerodynamic drag.
4. It must have satisfactory physical properties, such as sufficient strength, resistance to thermal shock (from rapid aerodynamic heating), resistance to rain erosion at high speeds, and minimum water absorption.

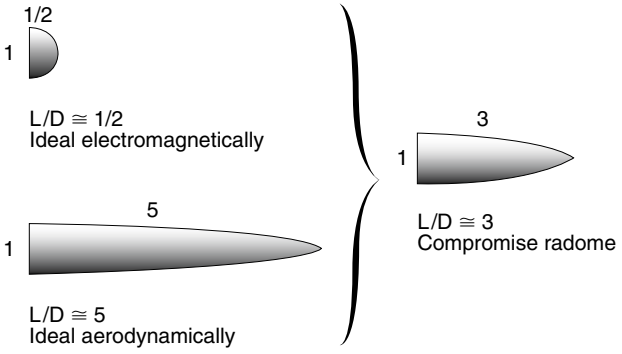

Figure 9. Three possible radome shapes are illustrated. For minimum angular distortion, a hemispherical shape (or hyperhemispherical shape as in a ground-based radar) would be ideal electromagnetically (upper left), but the drag penalty is excessive. From an aerodynamic perspective, the lower left radome shape is preferable, but it tends to have significant angular distortion characteristics. The tangent-ogive shape (on the right) is a typical compromise design. Nevertheless, some missiles use much blunter dome designs despite the drag penalty. L/D, lift-to-drag ratio.

As an example, Fig. 9 illustrates three conceivable radome shapes. The tangent-ogive shape (on the right) is a typical compromise design.

Guidance System Design Challenges

There are a significant number of challenges to designing guidance systems: the design must provide the desired performance while remaining robust to a multitude of error sources, limited control system bandwidth, and inherent system nonlinearities. Some of these challenges are summarized below.

1. The root-mean-square final miss distance from all deleterious noise sources must be minimized.
2. Guidance system stability must be maintained in the parasitic feedback loop (as mentioned above, this is caused by angular distortion of the radome/irdome). Radome angular distortion, in particular, is a key contributor to final miss distance but is considered separately from other noise sources as its impact on guidance system stability is substantial.
3. System nonlinearities must be avoided as much as possible; e.g., seeker gimbal angle and gyro rate saturations must be avoided, as should commanding missile acceleration beyond what is physically realizable by the missile.

Contributors to Final Miss Distance

With respect to guidance challenge item 1 above, there are a number of contributors to final miss distance (other than angular distortion of the radome/irdome). For example, in either an RF or IR guidance system, measurement noise from the various instruments (onboard

seeker, IMU, etc.) will tend to increase the final miss distance. In a radar-guided system, high illumination power on the target is desired in order to reduce the necessary receiver gain and, consequently, the internally generated noise. Similarly, a passive IR seeker is designed to have a maximum aperture size to maximize incoming power. Therefore, antenna/aperture size usually is made a maximum within the constraint of missile body diameter to maximize power reception and minimize angular beam width, thereby leading to less noise.

The ability for any given target sensor to resolve closely spaced objects also is limited, contributing to additional miss distance. For example, a missile radar antenna usually has a relatively wide beamwidth, and so it is unable to resolve closely spaced targets in angle until very late in the endgame of the engagement. In this sort of ambiguous situation, the homing missile can incur a large final miss distance.

Some of the key contributors to final miss distance are introduced below[8,11]:

1. Seeker receiver range-dependent angle noise, σ_{rd}. This noise is a function of the strength of the target return power and, hence, the signal-to-noise ratio. Range-dependent noise power varies inversely with range to target (R) as $1/R^2$ for semi-active radar and as $1/R^4$ for active radar. For IR systems, range-dependent angle noise typically is not considered to be a primary contributor.
2. Seeker range-independent angle noise, σ_{ri}. This noise is independent of target return power and is caused by a number of internal sources like signal processing and quantization effects, gimbal servo drive errors, and other electrical noise.
3. Scintillation (and glint) noise, σ_{glint}. These are coupled effects and are caused by target reflections that vary in amplitude and phase over time. (The effect is much like that of sunlight glinting from the shiny surfaces of an automobile.) Scintillation/glint noise can be very severe and is a function of the physical dimensions and motion of the target.
4. Clutter and multipath noise, σ_c. These noise effects become important at low altitudes, over either the land or sea. This noise is caused by the unwanted scattering (forward and backward) of radar returns from, for example, sea-surface waves.
5. Imperfect seeker stabilization caused by seeker gyro and gimbal scale factors, gyro drift, and missile body bending (flexing). Imperfect seeker stabilization can introduce parasitic feedback loops similar to that caused by radome/irdome distortion. The net effect can be viewed as inducing a bias or perturbation on the measured LOS rate. Exactly how these errors affect guidance performance will be a function of the way in which LOS reconstruction is mechanized.[9]
6. Initial heading errors at the start of homing. Heading error can be defined as the angle between the actual missile velocity vector at the start of terminal homing and the velocity vector that would be necessary to put the missile on an intercept course with the target. Heading error can be viewed as an initial condition disturbance to the guidance system at the start of terminal homing.
7. Target acceleration (maneuver) perpendicular to the LOS. A target can maneuver for any number of reasons (to avoid detection, to enact necessary course corrections, to evade a pursuing interceptor missile, etc.). Whatever the reason, from the viewpoint of the guided missile, target maneuver can have a stochastic quality to it and, in some instances, it can induce very large final miss distance. Relevant target maneuver (acceleration) levels and corresponding characteristics (horizontal weave, corkscrew, hard-turn, etc.) are key drivers to the design of missile guidance systems. Target maneuver generally is considered a (potentially significant) disturbance rather than noise to the guidance system.

Items 1–5 are stochastic noise sources, and the remaining items typically are referred to as non-noise contributors to final miss distance.

Radome/Irdome Refraction Error

The ogival shape of radomes helps to reduce drag but is a significant source of trouble to guidance system performance. Irdome shapes tend to be less problematic than radome shapes, but their effect on guidance system performance still must be considered. The fundamental issue is that as radiation passes through the dome, it is refracted by a certain angle which, in turn, depends on the seeker look angle, β. As illustrated in Fig. 10,[11] the radome distorts the boresight error measurement by an amount ε_{bse}. The magnitude of refraction during homing depends on many factors, including dome shape, fineness ratio, thickness, material, temperature, operating frequency, and polarization of the target return signal. Hence, it is very difficult to compensate perfectly for dome error *a priori*. Typically, the specification of dome characteristics involves the radome/irdome slope r (see Fig. 10), which is a local property of the dome and is defined as shown in Eq. 30:

$$r \equiv \frac{\partial \varepsilon_{bse}}{\partial \beta} . \tag{30}$$

Although r is not a constant over the entire dome, it can be regarded as constant over a small range of seeker look angles, β. The most optimistic situation is one in which the designer would be able to specify the manufacturing tolerances and, thus, the limits on the allowable variations of r.

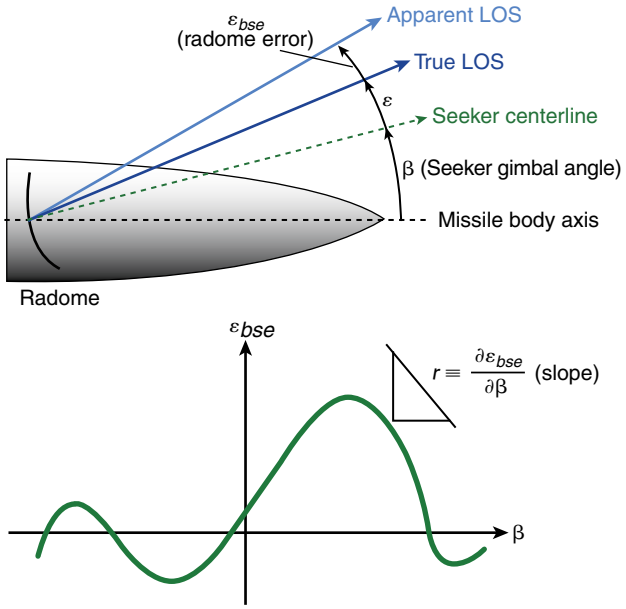

Figure 10. This illustration highlights the fact that the missile radome (or irdome) distorts the boresight error measurement. The boresight error distortion is a function of look angle.

Referring once again to Fig. 3, it follows that we can write the following angular relationship for the measured tracking error:

$$\varepsilon_m = \lambda + \varepsilon_{bse} - \theta . \tag{31}$$

Differentiating Eq. 31 and using the definition of radome slope shown in Eq. 30, we obtain the following expression for $\dot{\varepsilon}_m$:

$$\dot{\varepsilon}_m = \dot{\lambda} + \dot{\varepsilon}_{bse} - \dot{\theta} = \dot{\lambda} + r\dot{\beta} - \dot{\theta} . \tag{32}$$

Using the fact that the seeker dish angle can be written as $\theta = \psi + \beta$, we obtain the following expression for the derivative of the measured tracking error:

$$\dot{\varepsilon}_m = \dot{\lambda} - (1 - r)\dot{\beta} - \dot{\psi} . \tag{33}$$

Using Eq. 33, we can modify the block diagram shown in Fig. 5 to include the dome distortion effect (via Eq. 33). The result is shown in Fig. 11. Clearly, the boresight error creates another signal path in the missile guidance loop.

To obtain an alternate view of this parasitic loop and how it can affect guidance performance, we revisit Eq. 32. Referring to Fig. 3, we note that the seeker gimbal angle can be expressed as $\beta = \theta - \psi$ and that the measured LOS can be written as $\lambda_m = \theta + \varepsilon_m$. Also noting that it is typical for $|\mathbf{r}| << 1$, we can approximate Eq. 32 as

$$\dot{\lambda}_m \cong \dot{\lambda} - r\dot{\psi} . \tag{34}$$

Continuing, we also require transfer function descriptions of all components represented in Fig. 5. An approximate representation of the seeker block illustrated in Fig. 5 is given by the transfer function $G_s(s)$ below:

$$G_s(s) \triangleq \frac{s\theta(s)}{\lambda(s)} = \frac{s}{\tau_s s + 1} . \tag{35}$$

Directly from Fig. 5, the combined guidance system (filter and law) transfer function can be expressed as

$$G_g(s) \triangleq \frac{a_{Mc}(s)}{s\lambda(s)} = NV_c G_F(s) = \frac{NV_c}{\tau_f s + 1} . \tag{36}$$

Next, we assume the transfer function from commanded to achieved missile acceleration, $G_{FC}(s)$, can be

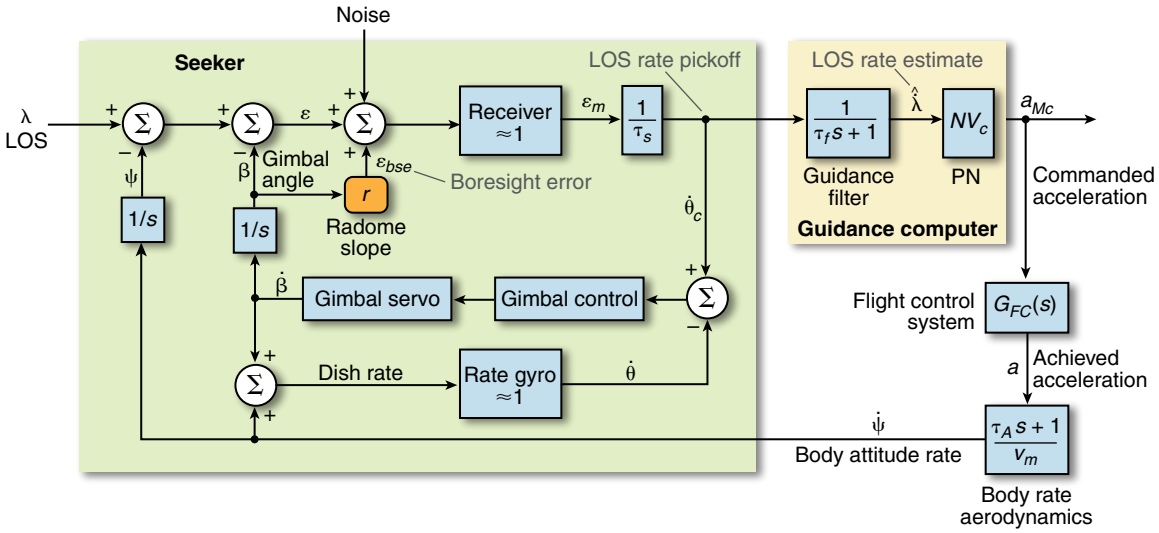

Figure 11. Simplified planar model of a gimbaled seeker track loop with the inclusion of radome/irdome distortion effects on the measured boresight error.

approximated by the following first-order lag representation:

$$G_{FC}(s) \triangleq \frac{a_M(s)}{a_{Mc}(s)} = \frac{1}{\tau_{FC}s + 1}. \quad (37)$$

Finally, recall that the missile aerodynamic transfer function from acceleration to body rate can be approximated as shown in Eq. 26 and repeated here for convenience:

$$G_A(s) \triangleq \frac{s\psi(s)}{a_M(s)} = \frac{\tau_A s + 1}{v_m}. \quad (38)$$

Using Eqs. 34–38, Fig. 5 can be drawn as illustrated in Fig. 12. Referring to this block diagram, the closed-loop transfer function from LOS rate to missile acceleration can be written as

$$G_R(s) \triangleq \frac{a_M(s)}{s\lambda(s)} = \frac{NV_c G_F(s) G_{FC}(s) G_s(s)/s}{1 + \dfrac{rNV_c G_A(s) G_F(s) G_{FC}(s) G_s(s)}{sv_m}}. \quad (39)$$

Static Effects

Without refraction ($r = 0$), the steady-state gain of the system in Eq. 39 is given by

$$g_{ss} \triangleq \lim_{s\to 0} G_R(s)\Big|_{r=0} = NV_c,$$

where recall that $N > 2$. On the other hand, if $r \neq 0$, then the steady-state gain of the system is given as

$$g_{ss} \triangleq \lim_{s\to 0} G_R(s)\Big|_{r\neq 0} = \frac{NV_c}{1 + r\dfrac{NV_c}{v_M}} \equiv \tilde{N}(r)V_c. \quad (40)$$

In Eq. 40, we have defined the resulting effective navigation ratio as $\tilde{N}(r) = N/(1 + rNV_c/v_M)$. Suppose the navigation ratio of the system is $N = 3$ (for the $r = 0$ case). Then, examining $\tilde{N}(r)$, if r is positive and (relatively) large and the ratio V_c/v_M increases beyond unity (as is often the case, particularly for near head-on engagements), then the effective navigation ratio $\tilde{N} \to 2$. Recall from the discussion of PN that a navigation gain of 2 or less will lead to guidance instability. This fact is illustrated in Fig. 13 for $N = 3$ and three different ratios of V_c/v_M. Conversely, when r is negative, the effective navigation ratio $\tilde{N}$ will increase, resulting in additional noise throughput, which also can have detrimental effects on guidance performance.

Dynamic Effects

It is shown in Ref. 4 that the guidance system transfer function given by Eq. 39 and illustrated in Fig. 12 can be approximated further by the following simplified transfer function:

$$G_R(s) \triangleq \frac{a_M(s)}{s\lambda(s)} \cong \frac{NV_c}{1+\rho}\frac{1}{1+s\tau_R}. \quad (41)$$

In Eq. 41, $\rho = rNV_c/v_M$, and the approximate overall time constant, τ_R, is given by the composite expression in Eq. 42:

$$\tau_R = \frac{(\tau_s + \tau_f + \tau_{FC}) + \rho\tau_A}{1+\rho}. \quad (42)$$

Referring to Eqs. 41 and 42, when the dynamic pressure is low (e.g., high altitudes and/or low missile velocity), the aerodynamic time constant τ_A tends to take on relatively large values (the missile turning rate becomes sluggish). For positive values of ρ, this effect is exacerbated and the missile guidance loop becomes even more sluggish. On the other hand, when the dynamic pressure is low, large negative values of ρ coupled with large τ_A can induce guidance instability.

As an example, consider Fig. 14, which illustrates the deleterious effects of radome-induced boresight error on homing guidance performance. This example uses PN guidance to guide the missile against a non-maneuvering target. No other noise sources are considered other than radome boresight error. Several curves are shown, each representing an autopilot response capability given by the time constant $\tau = \tau_{FC}$. Clearly, a more sluggish time constant exacerbates the effects of radome error slope on homing performance.

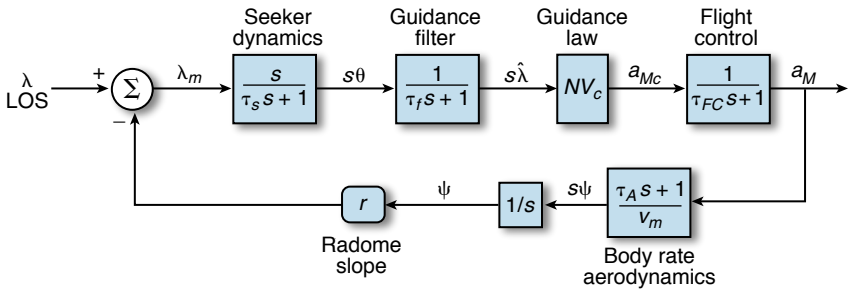

Figure 12. Alternate simplified block diagram of a (linear) missile guidance and control system that accounts for seeker dynamics, radome distortion, guidance filter effects, and autopilot/airframe response characteristics.

Guidance System Nonlinearities

In a guided missile, there are limits to the region of linear operation. For example, the lateral acceleration that a guided missile can attain is limited in one of two ways: (*i*) for low-altitude intercepts, structural considerations will limit the maximum acceleration levels, and (*ii*) for high-altitude intercepts, the

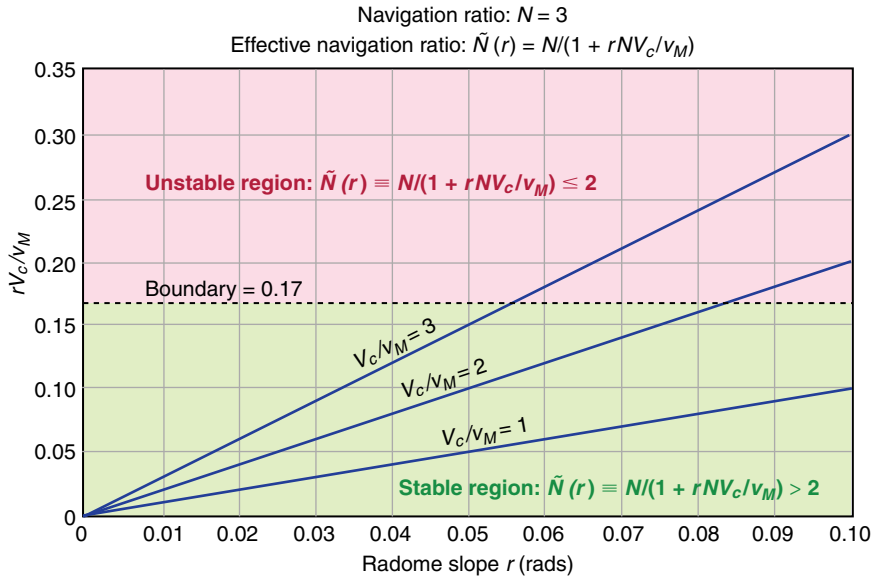
Navigation ratio: N = 3
Effective navigation ratio: Ñ (r) = N/(1 + rNVc/vM)
Unstable region: Ñ (r) ≡ N/(1 + rNVc/vM) ≤ 2
Boundary = 0.17
Vc/vM = 3
Vc/vM = 2
Vc/vM = 1
Stable region: Ñ (r) ≡ N/(1 + rNVc/vM) > 2
rVc/vM
Radome slope r (rads)

Figure 13. For a navigation ratio of 3, the effect of positive radome boresight error slope (*r*) for increasing ratios of closing velocity over missile velocity is shown. To maintain guidance stability, the effective navigation ratio must remain greater than 2.

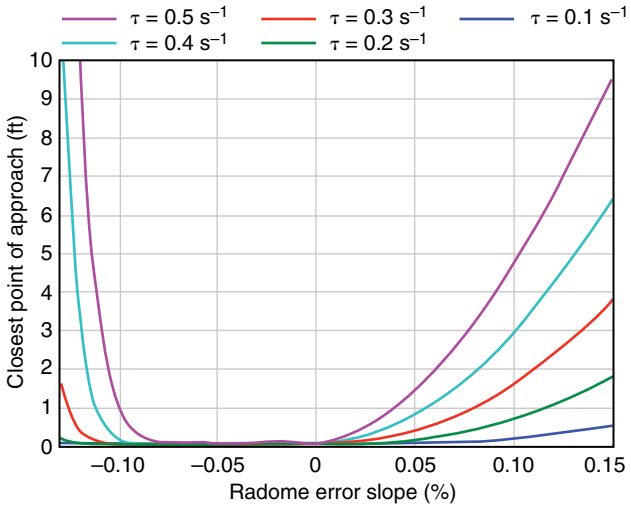

Figure 14. This plot illustrates the miss performance of PN versus radome boresight error slope. The results were derived by using a planar Simulink model assuming no error sources aside from radome error. Each curve represents the results using an autopilot with specified time constant τ. A larger time constant indicates a larger lag in the missile response to acceleration commands.

acceleration limit is more a result of maximum angle-of-attack limitations. In either case, the missile guidance and control system design must take the acceleration limits into account. The most significant implication is that the commanded acceleration from the guidance system must be hard-limited so as not to exceed the acceleration limits of the missile, which also implies that the flight control system (autopilot) must be designed to produce minimum overshoot to an acceleration step command. If/when the guidance command saturates, the missile guidance loop is essentially opened. If guidance command saturation persists long enough, and if this persistent saturation occurs near intercept, a significant final miss distance can result.

Missile seeker systems also are prone to nonlinear saturation, which can have significant deleterious effects on overall guidance performance. For example, on gimbaled platforms, the seeker gimbal angle can saturate under certain stressing conditions (e.g., while pursuing a highly maneuvering target). If this saturation occurs, the guidance loop has effectively become open and, if this occurs near intercept, significant final miss distance can occur.

Guidance Command Preservation

Three-dimensional guidance laws usually generate a guidance command vector without consideration to how the missile interceptor will effectuate the specified maneuver. For example, it is typical for a guided missile to (*i*) have no direct control over its longitudinal acceleration (e.g., axial thrust is not typically throttleable) and (*ii*) maneuver in the guidance direction (specified by the guidance law) by producing acceleration normal to the missile body. Therefore, the question naturally arises as to how a three-dimensional guidance command, specified by the guidance law without consideration of the aforementioned constraints, can be achieved by maneuvering the missile perpendicular to the missile centerline. We shall refer to this process as guidance command preservation.

In Ref. 1, two guidance command preservation techniques are developed. The first approach, referred to here as GCP1, is further elaborated in Ref. 12. The second guidance command preservation technique (GCP2) is a minimum norm solution. As such, GCP2 could (theoretically) provide savings in commanded acceleration (or fuel use in exoatmospheric applications) as compared with the first method. The GCP1 technique is discussed here.

GCP1 Technique

To describe this guidance command preservation technique, we refer to Fig. 15 and make the following

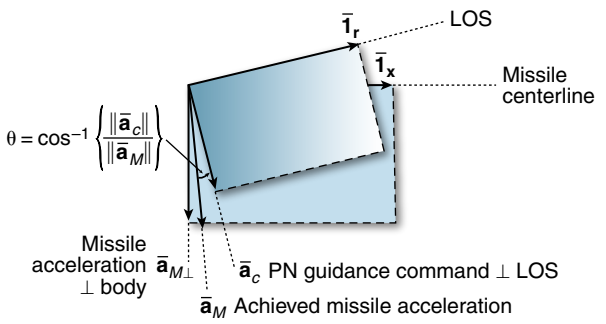

Figure 15. GCP1. The LOS vector is shown along with the commanded acceleration from PN, which is perpendicular to the LOS. Also, the missile centerline (direction of the missile nose) and achieved missile acceleration vector are superimposed. The guidance preservation problem is to achieve missile acceleration that has the component along the guidance direction as specified by the guidance law.

definitions: $\bar{1}_r$ is a unit vector along the missile–target LOS, $\bar{1}_x$ is a unit vector along the missile centerline (missile longitudinal axis), $\bar{a}_c$ is the guidance law acceleration command perpendicular to the LOS, and $\bar{a}_M = [a_{Mx} \quad a_{My} \quad a_{Mz}]^T$ is the achieved missile acceleration vector comprising components in the *x*/*y*/*z* axes.

Two component directions serve as a basis for the development of GCP1: the direction of the LOS ($\bar{1}_r$) and the commanded guidance direction ($\bar{1}_{a_c} = \bar{a}_c/\|\bar{a}_c\|$). Assuming perfect interceptor response to commanded acceleration (i.e., no lag from commanded to achieved acceleration), the (guidance preserved) missile acceleration can be expressed as follows:

$$\bar{a}_M = k_1\bar{1}_r + k_2\bar{1}_{a_c}. \tag{43}$$

The design parameters, k_1 and k_2 , are determined subject to the following constraints:

$$\begin{aligned}\bar{a}_M \cdot \bar{1}_x &= a_{Mx}\\ \bar{a}_M \cdot \bar{1}_{a_c} &= \|\bar{a}_c\|.\end{aligned} \tag{44}$$

Equations 44 analytically embody the following constraints: (*i*) the missile does not control longitudinal acceleration and (*ii*) the component of missile acceleration along the guidance direction, $\bar{1}_{a_c}$, must be that specified by the guidance law ($\bar{a}_c$). Using Eqs. 43 and 44 and given $\bar{1}_r \cdot \bar{1}_{a_c} = 0$ (i.e., the guidance command is perpendicular to the LOS), an expression for commanded missile acceleration that will preserve the guidance command is given in Eq. 45:

$$\bar{a}_{GL} = \left(\frac{a_{Mx} - \bar{a}_c \cdot \bar{1}_x}{\bar{1}_r \cdot \bar{1}_x}\right)\bar{1}_r + \bar{a}_c. \tag{45}$$

Equation 45 is derived independently from any particular coordinate system. It is easy to mechanize the expression in Eq. 45 such that the computations are carried out in the missile body frame (*B*). We first note that missile acceleration resolved into the missile body frame can be expressed as $\bar{a}_M^B = [a_{Mx}^B \quad a_{My}^B \quad a_{Mz}^B]^T$ and that the body-referenced unit vector along the longitudinal axis of the missile can be written as $\bar{1}_x^B = [1 \quad 0 \quad 0]^T$. The quantities $\bar{1}_r$ (LOS unit vector) and $\bar{a}_c$ (guidance law command) usually are defined with respect to a guidance reference frame. To reflect this fact, we express them as $\bar{1}_r^G = [1 \quad 0 \quad 0]^T$ and $\bar{a}_c^G = [0 \quad a_{cy}^G \quad a_{cz}^G]^T$. Here, the superscript denotes the frame of reference with which the quantities are currently expressed; in this case, the guidance reference frame (G). Thus, we must resolve all guidance frame quantities into the missile body frame through the coordinate transformation $\mathbf{C}_G^B = c_G^B(i,j)$, $i,j = 1,2,3$; for example, $\bar{1}_r^B = \mathbf{C}_G^B[1 \quad 0 \quad 0]^T \equiv [c_G^B(1,1) \quad c_G^B(2,1) \quad c_G^B(3,1)]^T$. Note that if we fix the guidance frame at the start of terminal homing ($t = 0$), we obtain the transformation $\mathbf{C}_I^G = \mathbf{C}_I^B(\mathbf{C}_B^S|_{t=0})$. The inertial-to-body transformation, $\mathbf{C}_I^B$, comes from the IMU, and $\mathbf{C}_B^S$ may be computed via the seeker gimbals (see Eq. 23). Subsequently, $\mathbf{C}_G^B = \mathbf{C}_I^B(\mathbf{C}_I^G)^T$. If necessary, the guidance frame may be updated from instant to instant, but this adds computational complexity. Given that $\mathbf{C}_G^B$ is available, the following mechanization of Eq. 45 is possible:

$$\begin{aligned}\bar{a}_{GC}^B &= \left(\frac{a_{Mx}^B - \bar{a}_c^B \cdot \bar{1}_x^B}{\bar{r}^B \cdot \bar{1}_x^B}\right)\bar{r}^B + \bar{a}_c^B\\ &\equiv \left(\frac{a_{Mx}^B - a_{cx}^B}{c_G^B(1,1)}\right)\begin{bmatrix}c_G^B(1,1)\\ c_G^B(2,1)\\ c_G^B(3,1)\end{bmatrix} + \begin{bmatrix}a_{cx}^B\\ a_{cy}^B\\ a_{cz}^B\end{bmatrix}.\end{aligned} \tag{46}$$

In Eq. 46, $[a_{cx}^B \quad a_{cy}^B \quad a_{cz}^B]^T$ is the guidance command vector expressed in the missile body frame. This mechanization will generate guidance commands in the missile body frame that satisfy the constraints in Eq. 44.

MIDCOURSE GUIDANCE

So far, this article has been chiefly concerned with the requirements of terminal homing, wherein target measurements are provided by one or more onboard terminal sensors and minimizing miss distance at intercept is the primary objective. For completeness' sake, we now will briefly discuss issues and requirements associated with the midcourse phase of flight.

During the midcourse guidance phase of a multimode missile (see Fig. 16), target tracking is performed by an external sensor to support the engagement.[6] External tracking relaxes the requirements for the onboard sensor to point at the target and detect it at large ranges.

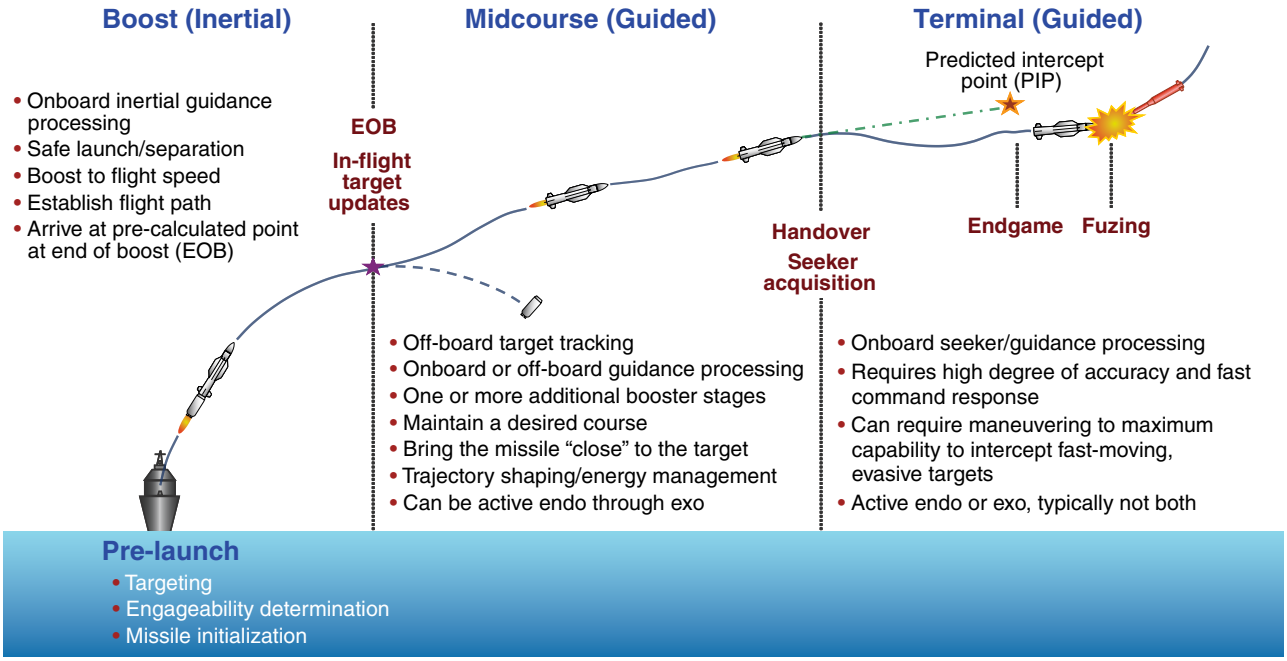
Boost (Inertial)
Midcourse (Guided)
Terminal (Guided)
• Onboard inertial guidance processing
• Safe launch/separation
• Boost to flight speed
• Establish flight path
• Arrive at pre-calculated point at end of boost (EOB)
EOB
In-flight target updates
Predicted intercept point (PIP)
Handover
Seeker acquisition
Endgame
Fuzing
• Off-board target tracking
• Onboard or off-board guidance processing
• One or more additional booster stages
• Maintain a desired course
• Bring the missile "close" to the target
• Trajectory shaping/energy management
• Can be active endo through exo
• Onboard seeker/guidance processing
• Requires high degree of accuracy and fast command response
• Can require maneuvering to maximum capability to intercept fast-moving, evasive targets
• Active endo or exo, typically not both
Pre-launch
• Targeting
• Engageability determination
• Missile initialization

Figure 16. Missile guidance phases. The weapon control system first decides whether the target is engageable. If so, a launch solution is computed and the missile is initialized, launched, and boosted to flight speed. Inertial guidance typically is used during the boost phase of flight during which the missile is boosted to flight speed and roughly establishes a flight path to intercept the target. Midcourse guidance is an intermediate flight phase whereby the missile receives information from an external source to accommodate guidance to the target. During the midcourse phase, the missile must guide to come within some reasonable proximity of the target and must provide desirable relative geometry against a target when seeker lock-on is achieved (just prior to terminal homing). The terminal phase is the last and, generally, the most critical phase of flight. Depending on the missile capability and the mission, it can begin anywhere from tens of seconds down to a few seconds before intercept. The purpose of the terminal phase is to remove the residual errors accumulated during the previous phases and, ultimately, to reduce the final distance between the interceptor and target below some specified level.

However, the accuracy of sensors generally degrades with distance. It is therefore unlikely that a standoff sensor will have sufficient accuracy in tracking both the target and missile to guide a missile close enough for intercept. The objectives during midcourse guidance are instead to guide the missile to a favorable geometry with respect to the target for both acquisition by the onboard sensor and handover to terminal homing.

During the midcourse guidance phase, the weapon control must provide information to the missile about the threat. This information may be nothing more than estimates of the threat kinematic states or may include a predicted intercept point (PIP). Predictions of the future target trajectory, whether calculated on board the missile or by the weapon control system, are based on assumptions of what maneuvers the threat is likely to do and what maneuvers are possible for the threat to perform. These assumptions typically are sensitive to the type of threat assumed but may include booster profiles, aerodynamic maneuverability, or drag coefficient(s). The PIP is therefore highly prone to errors. Occasional in-flight target updates may be needed to improve the accuracy of the PIP before handover to terminal homing.

A form of PN might be used during the midcourse guidance phase but generally results in excessive slowdown, however, as a result of the added atmospheric drag generated by maneuvers. Instead, it is desirable to use a guidance law that will maximize missile velocity during the endgame such that missile maneuverability will be maximized when called for during stressing endgame maneuvers. Lin[11] describes an approach that applies optimal control theory to derive efficient, analytical solutions for a guidance law that approximately maximizes the terminal speed while minimizing the miss distance. The guidance commands are expressed in the form given in Eq. 47:

$$a = \frac{K_1}{R} V^2 \sin(\delta)\cos(\sigma) - \frac{K_2}{R} V^2 \sin(\sigma) . \quad (47)$$

Here, V is the missile speed, R is the range to the PIP, δ is the angle difference between the current and desired final velocity, and σ is the heading error. The first term shapes the trajectory to achieve a desired approach angle to the intercept, and the second term minimizes miss. The gains K_1 and K_2 are time-varying

and depend on flight conditions, booster assumptions, and other factors. A critical component of implementing this law is computing an accurate estimate of time-to-go when the missile is still thrusting, which depends on the component of missile acceleration along the LOS. The guidance calculations can be made on board the missile or off board, with acceleration commands passed from the weapon control system to the missile where they are converted to body coordinates.

For exoatmospheric flight, drag is no longer an issue, but long flight times will result in curved trajectories as a result of gravity. From the current position, the Lambert solution (see Ref. 7 for a simple synopsis) defines the necessary current velocity to reach a terminal intercept point at a given time. A guidance law can be "wrapped around" the Lambert solution to progressively steer the missile velocity vector to align with the Lambert velocity. Then either thrust termination or a slowdown maneuver can be used to match the magnitude of the velocity of the Lambert solution when the missile booster burns out.

CLOSING REMARKS

The key objective of this article was to provide a relatively broad conceptual foundation with respect to homing guidance but also of sufficient depth to adequately support the articles that follow. First, we discussed handover analysis and emphasized that the displacement error between predicted and true target position, $\bar{\mathbf{e}}$, can be decomposed into two components: one along ($\bar{\mathbf{e}}_{\parallel}$) and one perpendicular to ($\bar{\mathbf{e}}_{\perp}$) the predicted LOS. Thus, because the relative velocity is along the LOS to the predicted target location, the error along this direction alters the time of intercept but does not contribute to the final miss distance. It is the error perpendicular to the LOS that must be removed by the interceptor after transition to terminal homing to effect an intercept.

Next, we developed a classical form of PN and noted that a primary advantage of PN, contributing to its longevity as a favored guidance scheme over the last five decades, is its relative simplicity of implementation. In fact, the most basic PN implementations require low levels of information regarding target motion as compared with other, more elaborate schemes, thus simplifying onboard sensor requirements. Moreover, it has proven to be relatively reliable and robust. This particular (and somewhat unique) treatment of PN was taken from a 1980 APL memorandum written by Alan J. Pue.[1] We also discussed how PN can be mechanized for guided missile applications, with a focus on LOS reconstruction and guidance command preservation. With respect to homing guidance, we itemized the primary contributors to guidance performance degradation that can ultimately lead to unacceptable miss distance.

The onboard missile seeker has a limited effective range beyond which target tracking is not possible. To support engagements that initially are beyond such a range, midcourse guidance is used to bring the missile within the effective range of the seeker. Thus, in contrast to terminal homing, during the midcourse guidance phase of flight, the target is tracked by an external sensor and information is uplinked to the missile. The key objectives during midcourse guidance are to guide the missile to a favorable geometry with respect to the target for both acquisition by the onboard missile targeting sensor and to provide acceptable handover to terminal homing. Many of the terminal homing concepts discussed here and in the subsequent articles on modern guidance and guidance filtering in this issue also are applicable to developing midcourse guidance policies. Thus, mainly for completeness, we briefly introduced the problem of midcourse guidance.

REFERENCES

[1] Pue, A. J., *Proportional Navigation and an Optimal-Aim Guidance Technique*, Technical Memorandum F1C(2)80-U-024, JHU/APL, Laurel, MD (7 May 1980).

[2] Ben-Asher, J. Z., and Yaesh, I., *Advances in Missile Guidance Theory*, American Institute of Aeronautics and Astronautics, Reston, VA (1998).

[3] Locke, A. S., *Principles of Guided Missile Design*, D. Van Nostrand Company, Princeton, NJ (1955).

[4] Shneydor, N. A., *Missile Guidance and Pursuit: Kinematics, Dynamics and Control*, Horwood Publishing, Chichester, England (1998).

[5] Shukala, U. S., and Mahapatra, P. R., "The Proportional Navigation Dilemma—Pure or True?" *IEEE Trans. Aerosp. Electron. Syst.* **26**(2), 382–392 (Mar 1990).

[6] Witte, R. W., and McDonald, R. L., "Standard Missile: Guidance System Development," *Johns Hopkins APL Tech. Dig.* **2**(4), 289–298 (1981).

[7] Zarchan, P., *Tactical and Strategic Missile Guidance*, 4th Ed., American Institute of Aeronautics and Astronautics, Reston, VA (1997).

[8] Stallard, D. V., *Classical and Modern Guidance of Homing Interceptor Missiles*, Raytheon Report D985005, presented at an MIT Dept. of Aeronautics and Astronautics seminar (Apr 1968).

[9] Miller, P. W., *Analysis of Line-of-Sight Reconstruction Approaches for SM-2 Block IVA RRFD*, Technical Memorandum F1E(94)U-2-415, JHU/APL, Laurel, MD (22 Dec 1994).

[10] Nesline, F. W., and Zarchan, P., "Line-of-Sight Reconstruction for Faster Homing Guidance," *AIAA J. Guid. Control Dyn.* **8**(1), 3–8 (Jan–Feb 1985).

[11] Lin, C. F., *Modern Navigation, Guidance, and Control Processing*, Prentice Hall, Englewood Cliffs, NJ (1991).

[12] Abedor, J. L., *Short Range Anti-Air Warfare Engagement Simulation*, Technical Memorandum F1E(86)U-3-031, JHU/APL, Laurel, MD (10 Nov 1986).

The Authors

Neil F. Palumbo is a member of APL's Principal Professional Staff and is the Group Supervisor of the Guidance, Navigation, and Control Group within the Air and Missile Defense Department (AMDD). He joined APL in 1993 after having received a Ph.D. in electrical engineering from Temple University that same year. His interests include control and estimation theory, fault-tolerant restructurable control systems, and neuro-fuzzy inference systems. Dr. Palumbo also is a lecturer for the JHU Whiting School's Engineering for Professionals program. He is a member of the Institute of Electrical and Electronics Engineers and the American Institute of Aeronautics and Astronautics. **Ross A. Blauwkamp** received a B.S.E. degree from Calvin College in 1991 and an M.S.E. degree from the University of Illinois in 1996; both degrees are in electrical engineering. He is pursuing a Ph.D. from the University of Illinois. Mr. Blauwkamp joined APL in May 2000 and currently is the supervisor of the Advanced Concepts and Simulation Techniques Section in the Guidance, Navigation, and Control Group of AMDD. His interests include dynamic games, nonlinear control, and numerical methods for control. He is a member of the Institute of Electrical and Electronics Engineers and the American Institute of Aeronautics and Astronautics. **Justin M. Lloyd** is a member of the APL Senior Professional Staff in the Guidance, Navigation, and Control Group of AMDD. He holds a B.S. in mechanical engineering from North Carolina State University and an M.S. in mechanical engineering from Virginia Polytechnic Institute and State University. Currently, Mr. Lloyd is pursuing his Ph.D. in electrical engineering at The Johns Hopkins University. He joined APL in 2004 and conducts work in optimization; advanced missile guidance, navigation, and control; and integrated controller design. For further information on the work reported here, contact Neil Palumbo. His email address is neil.palumbo@jhuapl.edu.

Neil F. Palumbo

Ross A. Blauwkamp

Justin M. Lloyd

The *Johns Hopkins APL Technical Digest* can be accessed electronically at **www.jhuapl.edu/techdigest**.

Overview of Missile Flight Control Systems

Paul B. Jackson

The flight control system is a key element that allows the missile to meet its system performance requirements. The objective of the flight control system is to force the missile to achieve the steering commands developed by the guidance system. The types of steering commands vary depending on the phase of flight and the type of interceptor. For example, in the boost phase the flight control system may be designed to force the missile to track a desired flight-path angle or attitude. In the midcourse and terminal phases the system may be designed to track acceleration commands to effect an intercept of the target. This article explores several aspects of the missile flight control system, including its role in the overall missile system, its subsystems, types of flight control systems, design objectives, and design challenges. Also discussed are some of APL's contributions to the field, which have come primarily through our role as Technical Direction Agent on a variety of Navy missile programs.

INTRODUCTION

The missile flight control system is one element of the overall homing loop. Figure 1 is a simplified block diagram of the missile homing loop configured for the terminal phase of flight when the missile is approaching intercept with the target. The missile and target motion relative to inertial space can be combined mathematically to obtain the relative motion between the missile and the target. The terminal sensor, typically an RF or IR seeker, measures the angle between an inertial reference and the missile-to-target line-of-sight (LOS) vector, which is called the LOS angle. The state estimator, e.g., a Kalman filter, uses LOS angle measurements to estimate LOS angle rate and perhaps other quantities such as target acceleration. The state estimates feed a guidance law that develops the flight control commands required to intercept the target. The flight control system forces the missile to track the guidance commands, resulting in the achieved missile motion. The achieved missile motion alters the relative geometry, which then is sensed and used to determine the next set of flight control

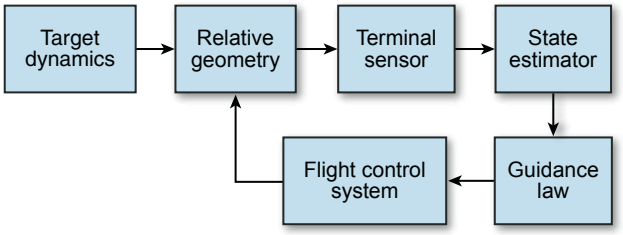

Figure 1. The flight control system is one element in the missile homing loop. The inertial missile motion controlled by the flight control system combines with the target motion to form the relative geometry between the missile and target. The terminal sensor measures the missile-to-target LOS angle. The state estimator forms an estimate of the LOS angle rate, which in turn is input to the guidance law. The output of the guidance law is the steering command, typically a translational acceleration. The flight control system uses the missile control effectors, such as aerodynamic tail surfaces, to force the missile to track steering commands to achieve a target intercept.

commands, and so on. This loop continues to operate until the missile intercepts the target.

In the parlance of feedback control, the homing loop is a feedback control system that regulates the LOS angle rate to zero. As such, the overall stability and performance of this control system are determined by the dynamics of each element in the loop. Consequently, the flight control system cannot be designed in a vacuum. Instead, it must be designed in concert with the other elements to meet overall homing-loop performance requirements in the presence of target maneuvers and other disturbances in the system, e.g., terminal sensor noise (not shown in Fig. 1), which can negatively impact missile performance.

The remainder of this article is divided into six sections. The first section discusses the specific elements of the flight control system. Particular emphasis is placed on understanding the dynamics of the missile and how they affect the flight control system designer. The next three sections describe different types of flight control systems, objectives to be considered in their design, and a brief design example. The last two sections discuss some of the challenges that need to be addressed in the future and APL's contributions to Navy systems and the field in general.

FLIGHT CONTROL SYSTEM ELEMENTS

As noted above, the flight control system is one element of the overall homing loop. Figure 2 shows the basic elements of the flight control system, which itself is another feedback control loop within the overall homing loop depicted in Fig. 1. An inertial measurement unit (IMU) measures the missile translational acceleration and angular velocity. The outputs of the IMU are

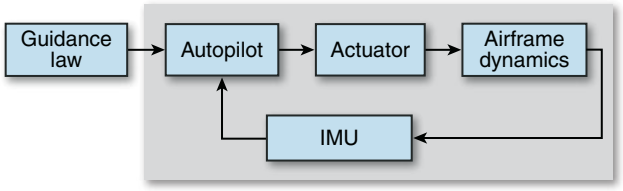

Figure 2. The four basic elements of the flight control system are shown in the gray box. The IMU senses the inertial motion of the missile. Its outputs and the inputs from the guidance law are combined in the autopilot to form a command input to the control effector, such as the commanded deflection angle to an aerodynamic control surface. The actuator turns the autopilot command into the physical motion of the control effector, which in turn influences the airframe dynamics to track the guidance command.

combined with the guidance commands in the autopilot to compute the commanded control input, such as a desired tail-surface deflection or thrust-vector angle. An actuator, usually an electromechanical system, forces the physical control input to follow the commanded control input. The airframe dynamics respond to the control input. The basic objective of the flight control system is to force the achieved missile dynamics to track the guidance commands in a well-controlled manner. The figures of merit (FOMs) used to assess how well the flight control system works are discussed in *Flight Control System Design Objectives*. This section provides an overview of each element of the flight control loop.

Guidance Inputs

The inputs to the flight control system are outputs from the guidance law that need to be followed to ultimately effect a target intercept. The specific form of the flight control system inputs (acceleration commands, attitude commands, etc.) depends on the specific application (discussed later). In general, the flight control system must be designed based on the expected characteristics of the commands, which are determined by the other elements of the homing loop and overall system requirements. Characteristics of concern can be static, dynamic, or both. An example of a static characteristic is the maximum input that the flight control system is expected to be able to track. For instance, a typical rule of thumb for intercepting a target that has constant acceleration perpendicular to the LOS is for the missile to have a 3:1 acceleration advantage over the target. If the missile system is expected to intercept a 10-*g* accelerating threat, then the flight control system should be able to force the missile to maintain a 30-*g* acceleration. An example of a dynamic characteristic is the expected frequency content of the command. For instance, rapid changes in the command are expected as the missile approaches intercept against a maneuvering threat, but the input commands may change more slowly during

the midcourse phase of flight where the objective is to keep the missile on an approximate collision path or to minimize energy loss. Other dynamic characteristics of concern include the guidance command update rate and the amount of terminal sensor noise flowing into the flight control system and causing unnecessary control actuator activity.

Airframe Dynamics

Recall that the objective of the flight control system is to force the missile dynamics to track the input command. The dynamics of the airframe are governed by fundamental equations of motion, with their specific characteristics determined by the missile aerodynamic response, propulsion, and mass properties. Assuming that missile motion is restricted to the vertical plane (typical for early concept development), the equations of motion that govern the missile dynamics can be developed in straightforward fashion.

Consider the diagram in Fig. 3, which shows the missile flying in space constrained to the vertical plane. The angle between the inertial reference axis and the missile velocity vector is called the flight-path angle γ. The angle from the velocity vector to the missile centerline is called the angle of attack (AOA) α. The angle from the inertial reference to the missile centerline is called the pitch angle θ. Acceleration in the direction normal to the missile A_z derives from two sources. The non-zero AOA generates aerodynamic lift. Normal acceleration also can be developed by a control input δ such as tail-fin deflection or thrust-deflection angle. In general, the missile acceleration also has a component along the centerline due to thrust and drag. For the simple model being developed here, we assume that this acceleration is negligible.

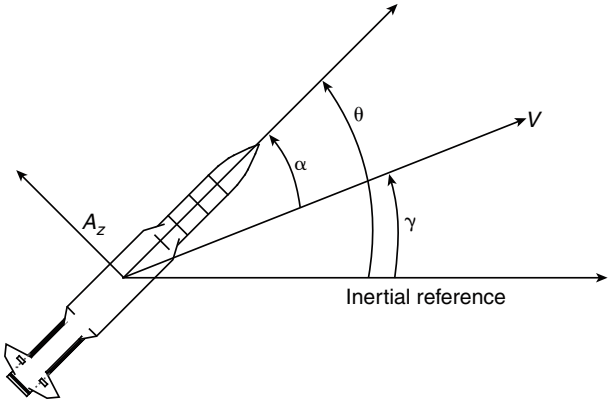

Figure 3. In the pitch plane, the missile dynamics and kinematics can be described by four variables. A_z is the component of the translational acceleration normal to the missile longitudinal axis. The AOA, α, is a measure of how the missile is oriented relative to the airflow and is the angle between the missile velocity vector and the missile longitudinal axis. The flight-path angle γ is a measure of the direction of travel relative to inertial space, i.e., the angle between the missile velocity vector and an inertial reference. The pitch angle θ defines the missile orientation relative to inertial space and is the angle between the inertial reference and the missile longitudinal axis.

Based on the diagram in Fig. 3, the fundamental relationship among the three angles above is

$$\alpha = \theta - \gamma \rightarrow \dot{\alpha} = \dot{\theta} - \dot{\gamma}. \tag{1}$$

The angular acceleration is the moment applied to the airframe divided by the moment of inertia,

$$\ddot{\theta} = \frac{M(\alpha, \delta)}{J}. \tag{2}$$

The applied moment is a function of the control input δ and the aerodynamic force induced by the AOA. The rate of change of the flight-path angle is the component of missile acceleration perpendicular to the velocity vector divided by the magnitude of the velocity vector. Assuming that the AOA is small, the flight-path angle rate is

$$\dot{\gamma} = \frac{A_z \cos(\alpha)}{V} \approx \frac{A_z}{V}. \tag{3}$$

The normal acceleration is determined by the forces applied to the missile divided by its mass

$$A_z = \frac{F_z(\alpha, \delta)}{m}. \tag{4}$$

The applied force is a function of the control input δ and the aerodynamic force induced by the AOA. Substituting Eqs. 3 and 4 into Eq. 1 and combining the result with Eq. 2 yields a coupled set of nonlinear differential equations where the state variables are the AOA and the pitch rate:

$$\begin{aligned} \dot{\alpha} &= \dot{\theta} - \frac{F_z(\alpha, \delta)}{mV} \\ \ddot{\theta} &= \frac{M(\alpha, \delta)}{J}. \end{aligned} \tag{5}$$

Although these differential equations can be solved numerically, an analytical approach often is desirable to fully understand the missile dynamics. Therefore, the equations of motion are linearized around an operating condition so that linear systems theory can be applied. Assuming constant missile speed, linearization of Eq. 5 yields a second-order state-space description of the missile dynamics

$$\begin{bmatrix} \dot{\alpha} \\ \ddot{\theta} \end{bmatrix} = \underbrace{\begin{bmatrix} -\frac{Z_\alpha}{V} & 1 \\ M_\alpha & 0 \end{bmatrix}}_{A} \begin{bmatrix} \alpha \\ \dot{\theta} \end{bmatrix} + \underbrace{\begin{bmatrix} -\frac{Z_\delta}{V} \\ M_\delta \end{bmatrix}}_{B} \delta$$
$$\begin{bmatrix} \dot{\theta} \\ A_z \end{bmatrix} = \underbrace{\begin{bmatrix} 0 & 1 \\ Z_\alpha & 0 \end{bmatrix}}_{C} \begin{bmatrix} \alpha \\ \dot{\theta} \end{bmatrix} + \underbrace{\begin{bmatrix} 0 \\ Z_\delta \end{bmatrix}}_{D} \delta, \quad (6)$$

where the numerical coefficients are defined by

$$Z_\alpha = \frac{1}{m}\frac{\partial F_z(\alpha, \delta)}{\partial \alpha}$$
$$Z_\delta = \frac{1}{m}\frac{\partial F_z(\alpha, \delta)}{\partial \delta}$$
$$M_\alpha = \frac{1}{J}\frac{\partial M(\alpha, \delta)}{\partial \alpha} \quad (7)$$
$$M_\delta = \frac{1}{J}\frac{\partial M(\alpha, \delta)}{\partial \delta}$$

and are evaluated at the particular operating condition of interest. Because these differential equations result from linearization around an operating point, the state, input, and output variables actually represent small signal perturbations around that operating point.

These linear differential equations apply for any missile under the stated assumptions. However, specific dynamics governed by these equations differ depending on the application. For example, for a tail-controlled endoatmospheric interceptor, the dynamics are a weak function of Z_δ. For a thrust-vector-controlled exoatmospheric interceptor, the aerodynamic forces are negligible and the terms Z_α and M_α can be set to zero.

The linear differential equations determine the dynamic behavior of the missile for small perturbations around the specified operating conditions. For example, suppose the missile is given an initial condition at an AOA a few degrees away from the nominal AOA around which the dynamics have been linearized. One important question is whether the missile will rotate back to the nominal AOA or diverge in the absence of any corrective control input. The answer to this question of stability is determined by the roots of the characteristic polynomial of the state matrix in Eq. 6:

$$s^2 + \frac{Z_\alpha}{V}s + (-M_\alpha) = 0\,. \quad (8)$$

A necessary and sufficient condition for both roots of this equation to have negative real parts and thus ensure stability is that all of the coefficients be positive. Using the conventions in Fig. 3, Z_α is always positive. Therefore, the stability of the missile in the absence of a control input is determined by the sign of M_α. If M_α is positive, the aerodynamic pitching moment forces the missile to diverge from the nominal AOA, and the missile is said to be statically unstable. If M_α is negative, the missile tends to be restored back to the nominal AOA, and the missile is said to be statically stable. The static stability of the missile is a crucial property that, under the stated assumptions, is determined solely by the sign of M_α, which is in turn determined by the aerodynamic configuration and the location of the missile center of mass.

Figure 4 illustrates in the complex *s*-plane how the roots of the characteristic equation migrate as a function of M_α. Again, for large, positive values of M_α, the missile is statically unstable, and the dynamics are governed by one unstable real root in the right half of the plane and one stable real root in the left half of the plane. As M_α decreases, the roots migrate toward the origin. When M_α is zero, the system has one real, stable root in the left half plane and one root at the origin. This condition is called neutral stability. As M_α becomes more negative, the roots migrate toward each other and eventually split apart as a complex pair.

The state-space representation in Eq. 6 describes the missile dynamics in the time domain. A representation in the complex frequency domain can be obtained that relates the input to the system, e.g., tail-deflection angle, to the system outputs, e.g., pitch rate and normal acceleration. This type of representation is called the trans-

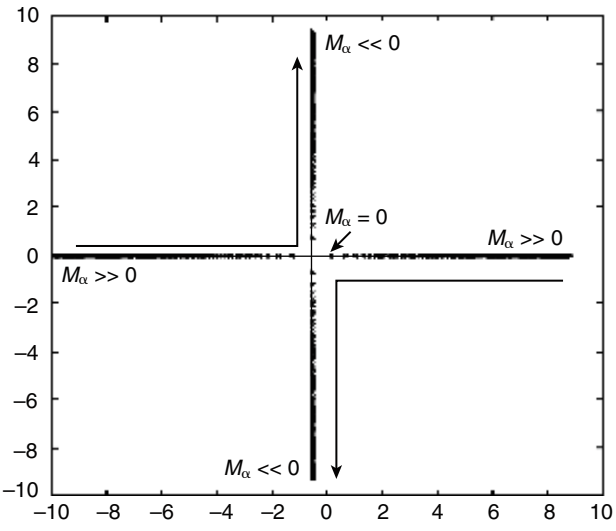

Figure 4. Static stability of the airframe is determined by the slope of the pitching moment curve with respect to the AOA, M_α. If the slope is positive, the missile is statically unstable because one of the roots of the characteristic polynomial of the governing differential equation is in the right half of the complex plane. If the slope is negative, both roots are in the left half of the plane and the missile is statically stable. The case where the slope is zero is called neutral stability, with one of the roots at the origin of the complex plane.

fer function and can be determined from the state-space model using the formula

$$H(s) = C(sI - A)^{-1}B + D, \quad (9)$$

where $s = \sigma + j\omega$ is complex frequency and A, B, C, and D are defined in Eq. 6.

In reality, missiles are not constrained to motion in a single plane. Figure 5 shows the relevant variables that describe the missile kinematics in three dimensions. The angle of sideslip (AOS) β is the yaw equivalent to the AOA. Together, they completely specify how the missile body is oriented relative to its velocity vector. The three components of the missile body angular velocity vector resolved in body-fixed coordinates are denoted p, q, and r, denoting the roll, pitch, and yaw rate, respectively. The pitch rate q was denoted as $\dot{\theta}$ in the discussion above where the motion was constrained to the pitch plane.

The equations that govern the dynamics of the missile can be developed by applying the Newton–Euler equations of motion. The translational motion can be described in terms of the derivatives of the AOA and the AOS. The rotational motion can be described in terms of the angular accelerations and takes a simple form assuming that products of inertia are zero:

$$\begin{aligned}\dot{\alpha} &= \cos^2\alpha\left(\frac{F_{zb}}{mu} - p\tan\beta + q\sec^2\alpha - \frac{F_{xb}}{mu}\tan\alpha - r\tan\alpha\tan\beta\right)\\ \dot{\beta} &= \cos^2\beta\left(\frac{F_{yb}}{mu} - r\sec^2\beta + p\tan\alpha - \frac{F_{xb}}{mu}\tan\beta + q\tan\alpha\tan\beta\right)\end{aligned} \quad (10)$$

$$\begin{aligned}\dot{p} &= \frac{M_{xb}}{Ix} - \frac{Iz - Iy}{Ix}qr\\ \dot{q} &= \frac{M_{yb}}{Iy} - \frac{Ix - Iz}{Iy}pr\\ \dot{r} &= \frac{M_{zb}}{Iz} - \frac{Iy - Ix}{Iz}pq.\end{aligned} \quad (11)$$

The lateral components of missile inertial translational acceleration resolved in body-fixed coordinates are

$$\begin{aligned}A_z &= \frac{F_{zb}}{m}\\ A_y &= \frac{F_{yb}}{m}.\end{aligned} \quad (12)$$

In these equations the forces and moments are resolved in body coordinates, with components indicated by the subscripts. Though not shown explicitly, all of the six components of the force and moment vectors are functions of the state variables and three control inputs, e.g.,

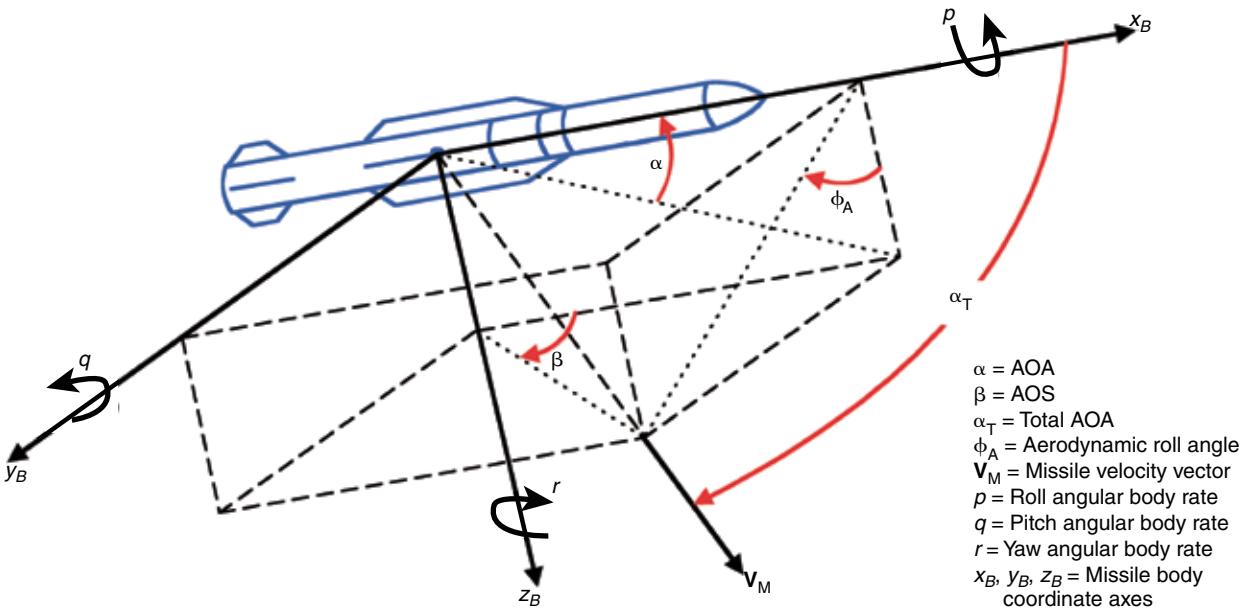

Figure 5. This diagram defines quantities used to describe the three-dimensional missile kinematics. Two angles are used to orient the missile relative to the velocity vector, either AOA and AOS or total AOA and aerodynamic roll angle. The components of the missile inertial velocity vector resolved in body-fixed axes are u, v, and w (not shown). The components of the inertial angular velocity vector resolved in body-fixed coordinates are p, q, and r. The missile orientation in inertial space usually is described via three Euler angles, typically in yaw–pitch–roll sequence (not shown).

$$F_{zb} = f(\alpha, \beta, p, q, r, \delta_p, \delta_y, \delta_r). \quad (13)$$

The dynamic equations together are a coupled, fifth-order, nonlinear differential equation. In situations where the mass properties vary with time, such as when a rocket motor is burning propellant, the differential equation is time-varying as well.

Equations 10–12 can be linearized around some operating condition of interest by expanding them in a Taylor series and retaining only the first-order terms. The result is a linear, time-invariant, state-space model with three inputs and five outputs:

$$\begin{aligned} \dot{x} &= Ax + Bu \\ y &= Cx + Du \\ x &= [\alpha \quad \beta \quad p \quad q \quad r]^T \\ u &= [\delta_p \quad \delta_y \quad \delta_r]^T \\ y &= [A_y \quad A_z \quad p \quad q \quad r]^T. \end{aligned} \quad (14)$$

As in the planar case, the state variables, control input variables, and output variables represent perturbations around the nominal operating condition.

Expanding the model to account for yaw and roll in addition to pitch brings a new set of challenges to the flight control designer. Foremost among these in many applications is aerodynamic cross-coupling as the total AOA increases, in which case aerodynamic surfaces on the leeward side of the missile become shaded by the fuselage, resulting in aerodynamic imbalances. The net effect typically results in undesirable motion, such as roll moment induced by a change in AOA or pitch moment induced by roll control input. The flight control system must compensate for these effects. An alternative is to simplify the airframe design to minimize cross-coupling, but the airframe must be designed with other factors in mind as well, such as maximizing the effective range of the missile. Compensating for aerodynamic cross-coupling for some missiles is challenging and often limits the maximum total AOA, and hence the maximum lateral acceleration, that can be achieved by the flight control system.

Actuator

The missile actuator converts the desired control command developed by the autopilot into physical motion, such as rotation of a tail fin, that will effect the desired missile motion. Actuators for endoatmospheric missiles typically need to be high-bandwidth devices (significantly higher than the desired bandwidth of the flight control loop itself) that can overcome significant loads. Most actuators are electromechanical, with hydraulic actuators being an option in certain applications. For early design and analysis, the actuator dynamics are modeled with a second-order transfer function (which does not do justice to the actual complexity of the underlying hardware),

$$\frac{\delta(s)}{\delta_c(s)} = \frac{\omega_a^2}{s^2 + 2\zeta_a \omega_a s + \omega_a^2}. \quad (15)$$

Although the actuator often is modeled as a linear system for preliminary design and development, it is actually a nonlinear device, and care must be taken by the flight control designer not to exceed the hardware capabilities. Two critical FOMs for the actuator for many endoatmospheric missiles are its rate and position limits. The position limit is an effective limit on the moment that the control input can impart on the airframe, which in turn limits the maximum AOA and acceleration. The rate limit essentially limits how fast the actuator can cause the missile to rotate, which effectively limits how fast the flight control system can respond to changes in the guidance command. The performance of a flight control system that commands the actuator to exceed its limits can be degraded, particularly if the missile is flying at a condition where it is statically unstable.

Inertial Measurement Unit

The IMU measures the missile dynamics for feedback to the autopilot. In most flight control applications, the IMU is composed of accelerometers and gyroscopes to measure three components of the missile translational acceleration and three components of missile angular velocity. For early design and analysis, the IMU dynamics often are represented by a second-order transfer function,

$$\frac{y_m(s)}{y(s)} = \frac{\omega_m^2}{s^2 + 2\zeta_m \omega_m s + \omega_m^2}, \quad (16)$$

for each rate and acceleration channel. Like the actuator, the IMU needs to be a high-bandwidth device relative to the desired bandwidth of the flight control loop. In some applications, other quantities also need to be measured, such as the pitch angle for an attitude control system. In this case, other sensors can be used (e.g., an inertially stabilized platform), or IMU outputs can feed strapdown navigation equations that are implemented in a digital computer to determine the missile attitude, which then is sent to the autopilot as a feedback measurement.

The flight control system must be designed such that the missile dynamics do not exceed the dynamic range of the IMU. If the IMU saturates, the missile will lose its inertial reference, and the flight control feedback is corrupted. The former may be crucial, depending on the specific missile application and the phase of flight. The

latter may be more problematic if the dynamic range is exceeded for too long, particularly if the missile is statically unstable.

Autopilot

The autopilot is a set of equations that takes as inputs the guidance commands and the feedback measurements from the IMU and computes the control command as the output. As mentioned previously, the autopilot must be designed so that the control command does not cause oversaturation of the actuator or the IMU. Because the autopilot usually is a set of differential equations, computing its output involves integrating signals with respect to time. Most modern autopilots are implemented in discrete time on digital computers, although analog autopilots are still used. The following section describes several types of autopilots that apply in different flight control applications.

TYPES OF FLIGHT CONTROL SYSTEMS

The specific type of flight control system that is implemented on a particular missile depends on several factors, including the overall system mission and requirements, packaging constraints, and cost. In many applications, the type of flight control system changes with different phases of flight. For example, the system used during the boost phase for a ground- or ship-launched missile could very well differ from the system used during the intercept phase. This section provides a brief overview of different types of flight control systems and when they might be used.

Acceleration Control System

One type of flight control system common in many endoatmospheric applications is designed to track commanded acceleration perpendicular to the missile longitudinal axis. In this system, deflection of an aerodynamic control surface, such as a tail fin, is the control input, and pitch angular rate (q) and acceleration (A_z) are measured by the IMU for feedback to the autopilot. The control deflection produces a small aerodynamic force on the tail fin but a large moment on the airframe because of its lever arm from the center of mass. The induced moment rotates the missile to produce the AOA, which in turn produces aerodynamic lift to accelerate the airframe.

Figure 6 represents equations that can be implemented in the autopilot to develop the commanded control surface deflection angle δ based on the commanded acceleration and feedback measurements of achieved acceleration A_z and pitch rate q. This particular structure can be found in many missile applications, but is by no means exclusive. As indicated in Fig. 6, the error between the commanded and achieved acceleration is used as an input to the inner control loops that control missile pitch rate. The pitch rate control loops include integration with respect to time that is implemented in circuitry for an analog autopilot or with numerical difference equations in a computer in a digital autopilot. The three control gains are selected so that the closed-loop flight control system has the desired speed of response and robustness consistent with other design constraints such as actuator limits. The autopilot in Fig. 6 is a reasonable starting point for a preliminary design. The final implementation would need to include other features, such as additional filters to attenuate IMU noise and missile vibrations, so that the system would actually work in flight and not just on paper.

Attitude Control System

Figure 7 shows another type of autopilot that can be used to control the attitude of the missile. In this case, the control effector is the thrust-deflection angle that is actuated by either a nozzle or jet tabs. The feedback loops have a structure similar to that used in the acceleration control system of Fig. 6, except that the outer loop is pitch-angle feedback instead of accelera-

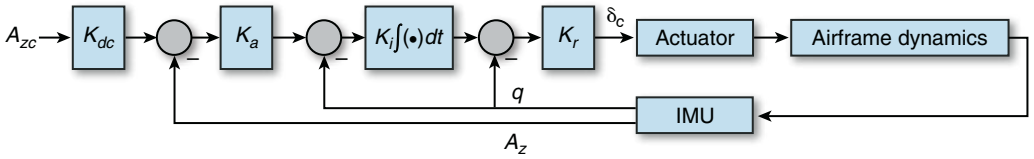

Figure 6. This block diagram illustrates a classical approach to the design of an acceleration control autopilot. The difference between the scaled input acceleration command and the measured acceleration is multiplied by a gain to effectively form a pitch rate command. The difference between the effective pitch rate command and the measured pitch rate is multiplied by a gain and integrated with respect to time. The resulting integral is differenced with the measured pitch rate and multiplied by a third gain to form the control effector command such as desired tail-deflection angle. The gain on the input acceleration command ensures zero steady-state error to constant acceleration command inputs. The final autopilot design would build on this basic structure with the addition of noise filters and other features such as actuator command limits. This basic structure is called the three-loop autopilot.

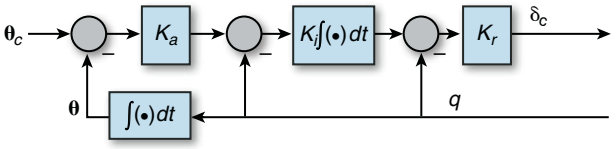

Figure 7. This attitude control system also has a three-loop structure like the acceleration control system. The difference lies in the selection of the numerical values of the gains to reflect a different design criterion, i.e., controlling attitude instead of acceleration.

tion. The numerical values of the gains in the control loops may differ for controlling attitude compared to controlling translational acceleration. The integration of pitch rate measured by the IMU to pitch attitude would typically be done via discrete integration in the missile navigation processing in the flight computer.

Flight-Path Angle Control System

Figure 8 shows an autopilot that can be used to track flight-path angle commands using thrust-vector control. This type of system assumes that aerodynamic forces are small and hence applies for exoatmospheric flight or for endoatmospheric flight when the missile speed is low. In this design, the feedback loops reflect the underlying physical relationships among the flight-path angle, AOA, flight-path angle rate, and pitch rate. The design explicitly uses estimates of the missile thrust and mass properties to compensate for how the missile dynamics change as propellant is expended. The commanded input into the autopilot is the desired flight-path angle. The output is the thrust-vector deflection angle. The feedback signals are the pitch rate q, flight-path angle rate $\dot{\gamma}$, AOA α, and flight-path angle γ. The pitch rate is measured by the IMU. The other feedback quantities are estimated in the missile navigation processing in the flight computer. This design is an example of the dynamic inversion design approach, which will be discussed in *Technology Development*.

FLIGHT CONTROL SYSTEM DESIGN OBJECTIVES

The particular FOMs used to evaluate the flight control system are application dependent. In this section, we explore typical FOMs that would generally apply. A specific application may include others as well.

Time-Domain Design Objectives

Flight control system FOMs can be expressed in the time and frequency domains. Figure 9 illustrates typical FOMs in the time domain. The plot shows the time response of the missile dynamics in response to a step change in commanded input. For example, this response could represent the achieved missile acceleration in response to a step change in commanded missile acceleration. The time constant and rise time characterize how quickly the system responds to the change in the command. The percentage overshoot and peak amplitude characterize the degree to which the response is well controlled. The steady-state error and settling time are indicators of how well the system tracks the desired command. As might be expected, designing the flight control system can require trade-offs between these FOMs. For example, a system that requires a small time constant may have to suffer larger overshoot.

In addition to time-domain requirements that measure how well the missile tracks the command in the desired plane of motion, the flight control system must be designed to minimize undesirable motion in response to that same command. For example, the missile should minimize motion in the horizontal plane in response to a guidance command in the vertical plane. In other words, the flight control system should "decouple the airframe," i.e., compensate for the natural aerodynamic coupling specific to the particular airframe in question. Decoupling is important insofar as the derivation of terminal guidance laws assumes a perfectly decoupled flight control system.

Frequency-Domain Design Objectives

Frequency-domain requirements are based on the classical control theory of Nyquist and Bode and are

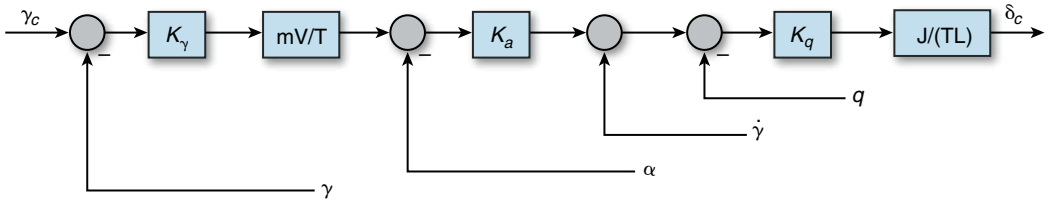

Figure 8. This diagram of a flight-path control system shows the dynamic inversion design approach. The design explicitly uses the fundamental relationships among the missile kinematic and dynamic variables as well as real-time estimates of the missile thrust and mass properties to naturally compensate for the changing missile dynamics as propellant is expended.

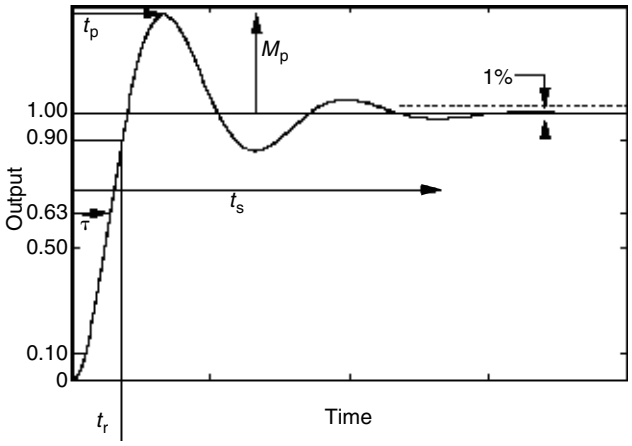

Figure 9. Some basic FOMs of a flight control system that are measured in the time domain are illustrated. These FOMs define how quickly the missile will respond to a change in guidance command and also the deviation of the achieved missile motion relative to the command (τ is time constant, M_p is peak magnitude, t_p is time to first peak, t_r is rise time, and t_s is settling time).

primarily concerned with quantifying the robustness of the flight control system. Robustness is important because the flight control system is designed based on models of the missile dynamics, actuator, and IMU, which are inherently approximations (i.e., no model is perfect). Qualitatively, robustness is the degree to which the flight control system can tolerate the error between the assumed models and the real system. Robustness can be addressed in several ways, two of which are discussed below. Classical stability margins quantify how much error can be tolerated at a single point in the system. More advanced techniques can be used to quantify robustness to simultaneous variations to multiple parameters in the model.

Classical Stability Margins

Two common measures of robustness are gain and phase margins as determined by an open-loop frequency response computed at a specific point of interest in the system. The open-loop frequency response is computed by breaking the loop at the point of interest and computing the frequency response of the negative of the transfer function from the resulting input to the resulting output (Fig. 10). The gain and phase as a function of frequency often

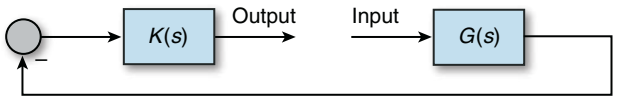

Figure 10. The open-loop transfer function at some point of interest is computed by "breaking the loop" at that point and computing the negative of the transfer function from the resulting input to the output. This open-loop transfer function is the bedrock of classical stability analysis in the frequency domain.

are plotted separately on what is called a Bode plot. Figure 11 is a Bode plot of an example open-loop frequency response for an acceleration control system with the loop broken at the input to the actuator. The gain margin is determined from the gain curve at the frequency where the phase crosses 180°. The gain margin tells how much the gain can be increased or decreased at the loop breakpoint before the closed-loop system becomes unstable. The phase margin is determined from the phase curve at the frequency where the gain curve crosses 0 dB. The phase margin tells how much extra phase lag, i.e., delay, can be tolerated at the loop breakpoint before the closed-loop system becomes unstable. Common requirements for gain and phase margins are 6 dB and 30°, respectively.

Mathematically, gain and phase margins only apply at the specific point for which they were computed. From an engineering standpoint, gain and phase variations need to be tolerated at many different points in the system. Qualitatively, the engineer needs to under-

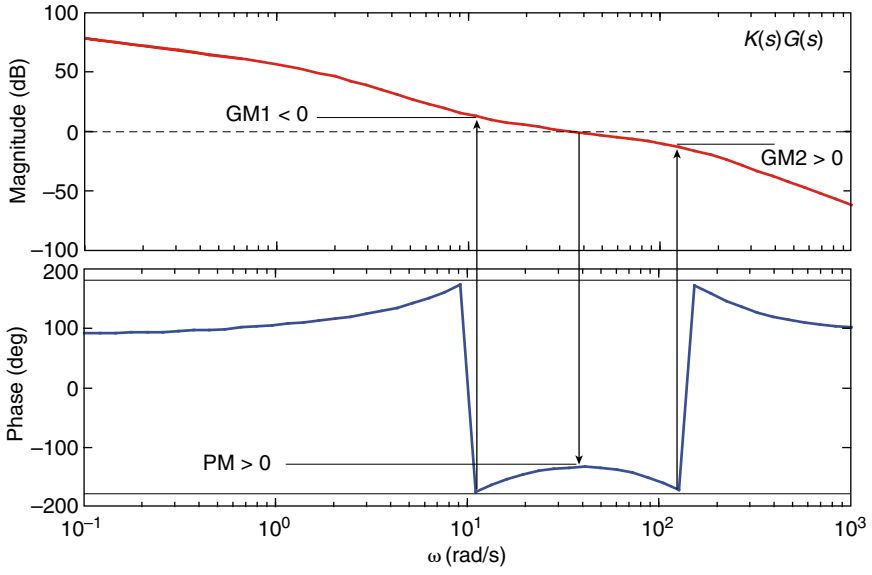

Figure 11. This Bode plot shows the open-loop frequency response of an acceleration autopilot with the loop broken at the input to the actuator. In this example, the missile is statically unstable, which results in the phase curve crossing the 180° line twice. The low-frequency crossover yields a decreasing gain margin (GM) and the high-frequency crossover yields an increasing GM. The gain curve crosses the 0-dB line between the phase crossover frequencies, resulting in a positive phase margin (PM). At high frequencies, the monotonically decreasing gain provides robustness to high-frequency modeling errors, uncertainty, and other effects.

stand how all of these variations can be translated to and combined at a single point. Consequently, designing for good gain and phase margins at a single point is an attempt to cover the net effect of all of the variability in the missile that the flight control system must tolerate. Typically, gain and phase margins are computed at the input to the actuator and also should be computed at the outputs of the IMU. In addition, gain and phase margins can be computed at other points in the system that may be of particular interest. For example, it may be useful to know how much M_α can be increased from its modeled value before the system becomes unstable.

The open-loop frequency response at the actuator shown in Fig. 11 exhibits characteristics common to a good design. At low frequencies, the gain is high, which is required for good command tracking, robustness to low-frequency variations from the modeled system dynamics, and rejection of low-frequency disturbances (e.g., a wind gust or a transient induced by a staging event). At high frequency, the gain is small and decreasing, which provides attenuation of high-frequency disturbances such as sensor noise and robustness to high-frequency variations to the modeled system dynamics, as discussed next.

At higher frequencies, the concept of gain and phase margins applies mathematically but is not as useful realistically because the models used for the design and analysis typically become increasingly inaccurate with increasing frequency because of the fundamental nonlinear nature of the system. Actuators, in particular, do not behave as linear systems at high frequency because of nonlinearities such as friction and backlash. Another issue is that missiles are not perfectly rigid. High-frequency flexible body vibrations in response to actuator motion can be sensed by the IMU and become a destabilizing effect. The net result is that predicted gain and phase values at high frequency can differ considerably from their actual values. A common approach to address this problem is to ensure that the open-loop gain is below some desired value at all frequencies above some certain lower bound. This approach desensitizes the system to high-frequency phase variations. The gain requirement is set based on assumptions about the high-frequency modeling errors, sometimes based on test data, and often comes from hard-learned experience. In general, the less the designer knows about the actual response of the system (relative to the modeled response), the more conservatism must be built into the design.

Not surprisingly, such conservatism comes at a cost. Gain and phase of a linear system across all frequencies must satisfy certain mathematical relationships and cannot be controlled independently. Therefore, the designer cannot decrease the gain at high frequency without also reducing the phase at lower frequencies, which then reduces the phase margin. Phase margin can be recovered by modifying the gain to move the 0-dB crossover point to lower frequencies, but this in turn will likely slow down the step response and increase the time constant. Conflicts between high-frequency attenuation requirements and low-frequency bandwidth requirements are not uncommon for a high-performance system, particularly with an unstable airframe, and can only be solved by giving up one for the other or re-addressing overall system requirements and the system configuration through systems engineering.

Robustness to Parameter Variations

So far the concept of robustness has been addressed through gain and phase margins, which apply at a single point or can be loosely thought of as "covering" simultaneous variations, and high-frequency attenuation, which covers high-frequency modeling errors and uncertainty. Another type of robustness that can be useful to quantify is tolerance to specific simultaneous parameter variations in the missile dynamics model, which is a more accurate error model than assuming that only one parameter can vary while holding the others fixed. For example, we might wish to know how much variability can be tolerated in M_α and M_δ simultaneously before the system becomes unstable.

This type of problem can be addressed by realizing that it can be viewed within the framework of Fig. 12. In Fig. 12, the transfer function matrix $M(s)$ represents the nominal, closed-loop flight control system, where w represents the guidance command (e.g., commanded acceleration), and z represents the achieved missile dynamics (e.g., achieved missile acceleration). The feedback matrix Δ represents the perturbation to the nominal system. In this example, Δ is a 2×2 diagonal matrix, with the diagonal elements representing the perturbations to the nominal values of M_α and M_δ. From the diagram, it is apparent that perturbations to the nominal system essentially act as an extra feedback loop. Hence, the question: *How big can Δ be before the feedback loop becomes unstable?*

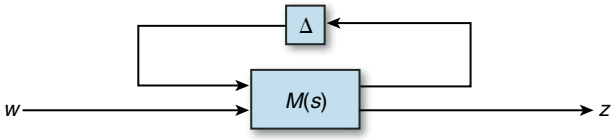

Figure 12. This block diagram illustrates a general way to represent the effect of modeling errors or uncertainty in a control system. Here, *w* represents the system input (e.g., an acceleration command), *z* is the system output (e.g., achieved acceleration), *M*(*s*) is the transfer function model of the nominal system, and Δ represents perturbations to the nominal parameters (e.g., moment of inertia or aerodynamic coefficients). The model uncertainty can be represented as the gain in a feedback loop around the nominal system. Because it is a feedback loop, stability of this system can be analyzed using feedback control theory.

One approach to answering this question is illustrated in Fig. 13. Conceptually, a stability boundary is defined by a locus of points in the ΔM_α–ΔM_δ plane. The goal is to find the minimum distance from the origin to the stability boundary. This constrained minimum distance problem can be solved numerically via a gradient projection search.[1] As with any gradient search, the problem of finding local minima must be addressed. This approach extends to problems of higher order, where the problem is to find the minimum distance from the origin of the perturbation space to an n-dimensional surface that defines the stability boundary.

Because the perturbations are really a feedback loop around the nominal system, another approach to addressing the simultaneous perturbation problem follows directly from stability theory for multi-input, multi-output feedback control systems. Using the maximum singular value $\bar{\sigma}$ for the measure of the magnitude of a matrix, the stability problem then is

$$\min_{\Delta}(\bar{\sigma}(\Delta)\,|\,s.t.\ \text{system is unstable}), \tag{17}$$

i.e., find the smallest perturbation matrix that destabilizes the system. The solution to this problem follows from the multivariable Nyquist stability theorem and actually is easily solved, assuming that the perturbation matrix Δ is a fully populated, complex matrix, when in reality it is a real, diagonal matrix. Hence, this approach tends to be conservative. In practice, much of the conservatism can be reduced by specifying in the minimization problem that the perturbation matrix has a specific structure

$$\min_{\Delta}(\bar{\sigma}(\Delta)\,|\,s.t.\ \text{system is unstable},\ \Delta \in \{\text{diagonal matrices}\})\ . \tag{18}$$

The additional constraint on the structure of the perturbation matrix makes this a much more difficult problem to solve.

Although the simultaneous perturbation problem can be solved mathematically, the flight control engineer still needs to formulate the problem in a meaningful way, particularly when dealing with perturbations to parameters that can have very different dynamic ranges or even different physical units. Hence, determining the appropriate scaling on the perturbed parameters is an important first step in these types of problems.

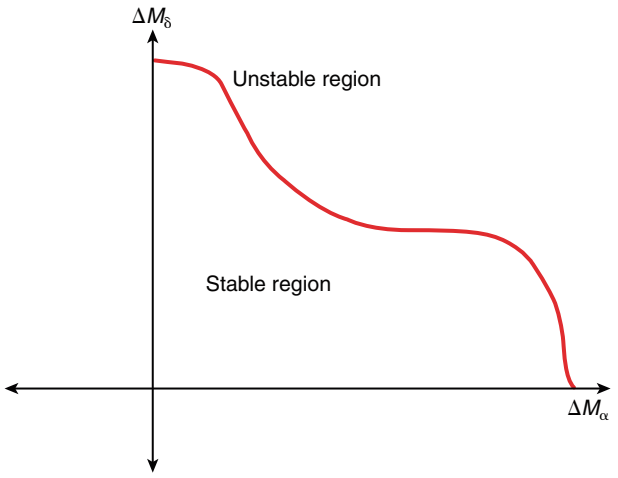

Figure 13. The stability of the perturbed system can be represented by regions in the perturbation plane. The analysis problem then is to define the stability boundary and the shortest distance from it to the origin. This problem can be solved with a projected gradient search. This solution approach extends to more than two perturbations and can even be used with complex perturbations that represent changes in both gain and phase at critical points in the system.

PITCH ACCELERATION AUTOPILOT EXAMPLE

This section presents an example of a pitch acceleration autopilot design for a tail-controlled missile and illustrates some of the FOMs discussed above.

The missile dynamics have been linearized around a nominal operating condition of a 10° AOA and a missile speed of Mach 3. Evaluating the slopes in Eq. 7, inserting them into the state-space model, and computing the transfer functions in the frequency domain yields

$$\begin{aligned}\frac{A_z(s)}{\delta(s)} &= \frac{0.2038(s^2 - 34.3^2)}{s + 0.56 \pm 9.32j}\\ \frac{q(s)}{\delta(s)} &= \frac{-131(s+1)}{s + 0.56 \pm 9.32j}\ .\end{aligned} \tag{19}$$

The denominator of these transfer functions is the same as the left-hand side of the characteristic equation in Eq. 8. At this condition, the missile has a stable airframe with a pair of lightly damped complex poles.

This example assumes that the tail-fin actuator dynamics can be represented by a second-order transfer function (e.g., Eq. 15) with $\omega_a = 150$ rad/s and $\zeta_a = 0.7$. The IMU is assumed to be ideal, i.e., the feedback measurements are equal to their corresponding true values.

The autopilot for this example is the basic three-loop autopilot shown in Fig. 6. The autopilot gains are selected to provide a time constant of less than 0.2 s with minimal overshoot. The resulting autopilot gains are $K_{dc} = 1.1$, $K_a = 4.5$, $K_i = 14.3$, and $K_r = -0.37$.

The achieved missile acceleration in response to a unit-step acceleration command input is shown in Fig. 14. The time constant is approximately 0.18 s, and the overshoot is only a few percent. The response in Fig. 14 shows that the initial acceleration develops in the negative direction before reversing and eventually

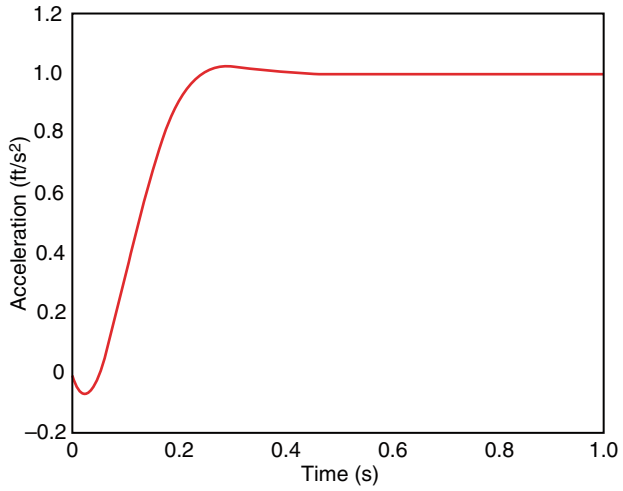

Figure 14. The response to a unit-step input acceleration command for the pitch acceleration control system example is shown. This response illustrates the characteristics of a good design, such as a small time constant, small overshoot, and zero steady-state error. The initial acceleration in the negative direction is common to tail-controlled missiles.

tracking the command. This feature is common to tail-controlled missiles. The tail must develop a negative force at the aft end of the missile in order to pitch the nose up and develop a positive AOA. The initial negative kick by the tail moves the center of gravity in the negative direction before the AOA increases and develops positive lift to accelerate the missile in the desired direction.

Figure 15 shows the Bode plot of the open-loop frequency response with the loop broken at the actuator. The gain and phase margins are indicated on the plot and at first glance appear to meet the classical criteria of 6 dB and 30°, respectively. However, the true gain and phase margins might be considerably lower once other effects are included in the model, such as IMU dynamics and measurement latencies as well as time delays associated with the digital implementation of this autopilot in the flight computer. The Bode plot also shows another desirable aspect of a good design: the gain curve is monotonically decreasing at high frequencies, which provides some robustness against unmodeled high-frequency dynamics, such as the aforementioned flexible body vibrations.

TECHNOLOGY CHALLENGES

In this section, we review the classical approach to designing missile flight control systems and discuss where improvements are needed as the requirements on the flight control system become more stringent to pace the threat.

The classical approach to designing the missile flight control system can be summarized as follows.

1. Develop linear models of the actuator and sensor.
2. Define the functional form of the autopilot equations.
3. Develop a linear model of the missile dynamics at a flight condition of interest.
4. Design autopilot gains in the pitch, yaw, and roll channels, assuming an aerodynamically decoupled airframe to meet basic time-domain requirements.
5. Design additional compensation for aerodynamic cross-coupling.
6. Design additional filters to attenuate sensor noise and flexible body vibrations.
7. Assess linear robustness and performance of the fully coupled system.
8. Return to 4 if necessary.
9. Repeat 3–8 for all flight conditions of interest.
10. Develop a methodology to smoothly transition from one set of gains to the next as the missile flies through different flight conditions.
11. Add nonlinear features, such as actuator command limits, if necessary.

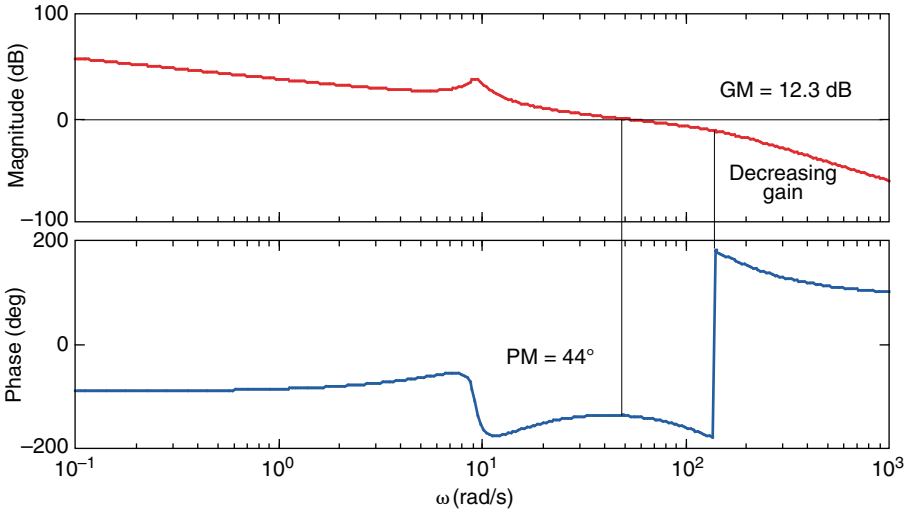

Figure 15. The Bode plot with the loop broken at the actuator input for the example pitch acceleration control system shows the characteristics of a good design. The gain is high at low frequency and low at high frequency. The stability margins are high. These margins will be reduced as other effects are included in the analysis, such as IMU dynamics and flight computer processing computational delay.

12. Evaluate in a high-fidelity simulation using nonlinear aerodynamic, actuator, and sensor models.
13. Return to 3 if necessary.

This approach has worked well in the past and will continue to work well in the future for many applications. However, for high-performance interceptors that need to achieve a high AOA with a small time constant, this approach can suffer. One potential problem is the separate steps in 4 and 5 for dealing with the aerodynamic coupling. Intuitively, it might be expected that designing the in-channel and cross-coupling compensation in a unified design approach would yield superior performance. Another area for improvement is the way in which the high-fidelity models are used only for assessment after the basic design is complete. As required time constants decrease, the autopilot will likely saturate the actuator for longer periods of time, suggesting that nonlinear simulation may need to be integral to the design process. Further complicating the design is that steps 3–8 might need to be carried out for thousands of operating conditions.

As the classical design approach evolves, the following challenges need to be addressed:

- The design approach should account for hardware nonlinearities as a fundamental element of the design process.
- The design approach needs to be easily automated so that computer programs can be written to design the autopilot gains over the entire flight envelope to minimize the need for "design by hand."
- The design approach should work directly on the fully coupled model of the missile dynamics.
- A good design approach should yield a design that is easily adaptable to changes in the missile configuration, specifically the mass properties that tend to change over the course of a missile development and production program.

Though not explicitly stated, any desirable design method should yield a robust control system when properly applied.

The first challenge can be addressed by designing the autopilot using numerical optimization programs. The cost function that is optimized can include many if not all of the FOMs previously discussed, including those from the time-domain response as determined from high-fidelity simulations that include models of the system hardware with their nonlinear dynamics. In this way, the trade-off between robustness and nonlinear time response is brought directly into the process. The challenge then becomes developing a cost function that will meet engineering design goals when it is optimized. The last three challenges can be addressed through the selection of the specific design method to apply to any particular system. Many control system design techniques are available, but finding one method that meets all three of these criteria is difficult. APL's contributions in this area are addressed in the next section.

APL CONTRIBUTIONS

APL has been involved in the development of flight control systems for the Navy since the earliest missiles were being developed. For many of these programs, APL serves as the Technical Direction Agent and, as such, provides support over the life cycle of a missile program. APL also evaluates new theoretical developments in control theory for their applicability to the missile flight control design problem.

Life Cycle Support

During the concept development phase of a program, APL is involved in developing the requirements for the flight control system. These requirements then flow down to subsystem requirements on the airframe, actuator, and IMU. Typically, this subsystem flow-down requires some level of an autopilot design to demonstrate the feasibility of the entire system meeting the flight control requirements.

As the missile program proceeds to the development phase, APL works closely with the design contractor to ensure a robust design that meets requirements. APL develops models, independent of the contractor, that can be used for model verification and performs an independent assessment of the design. This assessment includes linear analyses as well as predictions from high-fidelity time-domain simulations. Parts of the analyses may replicate those performed by the contractor to verify results. The results of these analyses are communicated back to the contractor with emphasis on areas of concern and potential solutions that may need to be addressed in a subsequent design iteration.

As the program progresses to the test-flight phase, APL works with the contractor and other organizations to develop test objectives and scenarios. The scenarios are designed to maximize coverage over the design space and demonstrate flight control performance, with particular emphasis on the time constant and maximum acceleration. Along with scenario development are preflight predictions based on high-fidelity simulations. After the flight, APL again conducts an independent postflight analysis and also uses the flight test data for model validation.

Technology Development

In addition to supporting missile development programs, APL has taken an active role in applying new

theoretical developments in the field of control systems design and assessing their applicability to the missile flight control design problem. Our particular emphasis has been on addressing the last three challenges listed previously, i.e., developing design methods that can be automated, apply to the fully coupled pitch–yaw–roll dynamic model, and are adaptable to changes in the missile configuration. This activity has been ongoing since the earliest Navy missile programs. This article covers only the relatively recent activities over the last 20 years or so.

In the late 1980s, APL demonstrated that the linear quadratic regulator (LQR) theory can be applied to the missile autopilot design problem. The LQR design problem is to find the control input that minimizes a quadratic function of the state and control

$$C = \int_0^\infty (x^T Q x + u^T R u)\, dt\,, \tag{20}$$

where x is the vector of state variables—e.g., AOA, AOS, etc.—and u is the vector of control inputs—e.g., pitch, yaw, and roll tail deflections. The constant, symmetric weighting matrices, Q and R, must be selected to reflect the desired time-domain design criteria, such as time constant and overshoot. The primary benefit of the LQR approach is that the control solution typically has very good stability margins. The difficulty had always been in the appropriate selection of Q and R to represent engineering design criteria. APL used the theoretical work of Harvey and Stein,[2] where Q and R can be constructed to specify a desired eigenstructure of the closed-loop control system. The closed-loop eigenvalues can be specified based on time-domain requirements, and the eigenvectors can be specified to reflect the desired degree of decoupling between the control channels. This approach has been demonstrated to yield robust designs based on the fully coupled dynamic model and can be automated to work on all flight conditions across the battle space. It does not, however, easily adapt to changes in the missile configuration. Such changes typically require another iteration of the design over the entire design space.

The late 1980s and early 1990s saw an explosion in the use of so-called H_∞ design techniques, primarily as a result of the groundbreaking solution of the control problem indicated in Fig. 16.[3] In the frequency domain, the mathematical objective is to find the controller $K(s)$ to compute the control u based on measurements y from the plant $P(s)$ that minimizes the infinity norm of the transfer function matrix that relates the inputs w to the outputs z. The infinity norm of a transfer function matrix is defined as

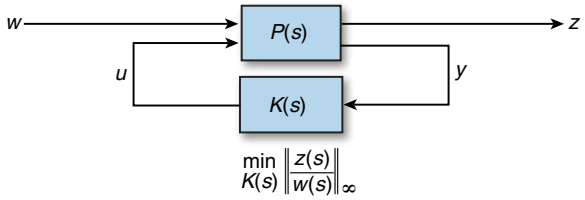

Figure 16. The H_∞ design problem is to find the controller $K(s)$ that minimizes the infinity norm of the transfer function from the inputs in vector w to the outputs in vector z. For the flight control design problem, the plant $P(s)$ models the actuator, airframe, and IMU dynamics. The controller $K(s)$ is the frequency-domain representation of the autopilot. The inputs w are the guidance commands and the outputs z are frequency-weighted signals, such as the achieved acceleration. The frequency-dependent weights can be chosen to represent typical time-domain and frequency-domain design objectives. An approximate solution to this problem can be reached through an iterative approach and involves the solution of two algebraic Riccati equations for each iteration.

$$\left\| H(s) \right\|_\infty = \sup_{\omega = 0 \to \infty} \bar{\sigma}(H(j\omega))\,. \tag{21}$$

Loosely speaking, the infinity norm is a measure of the maximum gain from input to output over all frequencies.

For the flight control application, the plant represents the missile dynamics, actuator, and IMU. The controller is the autopilot. The control u is the actuator command, and the measurements y are the IMU outputs. The inputs w would include, for example, pitch and yaw acceleration commands, and the outputs z would include the pitch and yaw acceleration errors and the missile roll rate. The key is that the outputs are not the actual signals themselves but frequency-weighted versions of those signals. The frequency-dependent weights map time and frequency-domain design goals to the peak gain over all frequencies of the transfer function from w to z.

This approach works well for designing missile autopilots at specific operating conditions based on a fully coupled model of the missile dynamics. However, it results in high-order controllers that may be difficult to implement, and it is not easy to automate over the design space. APL pioneered the use of this method for the autopilot design problem. Some of this work is contained in Refs. 4–9.

In the early-to-mid-1990s, APL took the lead on the Highly Responsive Missile Control System Advanced Technology Demonstration program. This program had several objectives, one of which was to demonstrate the efficacy of modern design techniques for the flight control problem and show that the resulting design could be implemented in real time on an embedded processor.

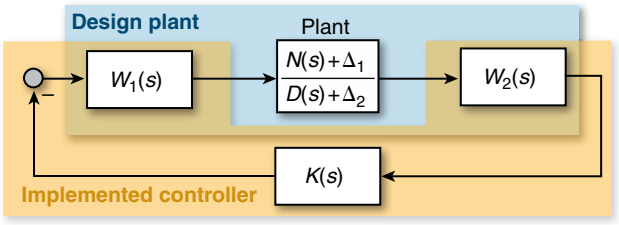

Figure 17. The normalized co-prime factorization approach uses frequency-dependent weights to shape the open-loop frequency response. The design problem is to solve for the controller $K(s)$ to achieve the desired open-loop response and simultaneously maximize robustness to uncertainty in the numerator and denominator of the transfer function that models the plant dynamics. The weights $W_1(s)$ and $W_2(s)$ are treated as part of the plant for designing $K(s)$ and then appended to $K(s)$ for the controller that is implemented in the missile software.

The design method used in this program was based on the normalized, co-prime factorization (NCF) approach.

In the NCF approach, the plant in the frequency domain is viewed in terms of a transfer function numerator and denominator ($N(s)$, $D(s)$), where each has some associated uncertainty, as in Fig. 17. The control problem is to find the controller $K(s)$ to achieve the desired open-loop frequency response specified by the weighting functions $W_1(s)$ and $W_2(s)$ and simultaneously maximize the size of the uncertainty that would result in an unstable system. The weighting functions are specified by the designer as part of the plant model in the design step and then combined with $K(s)$ for implementation. Examples using this approach can be found in Ref. 10.

The NCF approach was shown to yield solid, robust designs and could be automated across the design space. However, a completed design does not readily adapt to changes in the missile configuration. Also, it does yield high-order controllers that can be difficult to implement. Unfortunately, the effort was halted before it could be shown that the resulting design could be implemented in real time.

In the mid-1990s, APL was involved in the analysis of various missile system concepts being proposed for the tactical ballistic missile defense mission. To assess these concepts, APL developed weapon system simulations to evaluate predicted performance. Although none of the conceptual systems had actually been designed at this point, the Navy nevertheless desired that the simulations be of relatively high fidelity. To this end, APL had to design prototype flight control systems that could be used in high-fidelity, nonlinear, launch-to-intercept simulations that used fully coupled aerodynamic models. These prototype designs had to be developed reasonably quickly, be easily modified to adapt to weight and center-of-mass changes to each concept, and represent the expected tactical performance of each of these concepts.

To this end, APL used a technique called nonlinear dynamic inversion to quickly design prototype flight control systems. At its core, this technique is very simple, yet it is a powerful design approach. Consider the nonlinear system that is affine in the control input,

$$\dot{x} = f(x) + g(x)u\,. \tag{22}$$

The control u is to be designed such that the system dynamics follow some desired trajectory that is a function of the state and commanded state,

$$\dot{x}_d = h(x, x_c)\,. \tag{23}$$

A typical form for the desired dynamics is a first-order lag,

$$h(x, x_c) = \frac{x_c - x}{\tau}, \tag{24}$$

with τ being the desired time constant. These desired dynamics can be achieved through a feedback control law of the form

$$u = g^{-1}(x)(h(x, x_c) - f(x))\,, \tag{25}$$

assuming that the state vector can be measured.

For the acceleration autopilot design problem, for example, the dynamic inversion actually is used twice. First, it is applied to develop control of the missile pitch rate given a desired pitch rate command. Once the pitch rate control loop is designed, it becomes part of the effective plant for which the outer acceleration control loop is defined, using the guidance acceleration command as the reference input.

The dynamic inversion design approach is appealing. It is a simple concept to understand and apply. Because the missile dynamics are explicitly part of the control law, it is easily automated and works directly on the nonlinear, fully coupled pitch–yaw–roll dynamic model. A direct consequence is that the autopilot design naturally adapts to modifications in the missile configuration. For example, a change to the missile mass properties can be naturally accommodated by updating values in the computations of $f(x)$ and $g(x)$ in Eq. 25, whereas for the autopilot shown in Fig. 6, the relationship between the values of each gain and the mass properties will not be readily apparent.

The primary drawback of the dynamic inversion approach is that is does not provide any theoretical guarantees of robustness. Instead, it relies on an experienced designer to specify desired dynamics that can be reasonably achieved by the airframe and within the bandwidth constraints of the system hardware. As with any design

approach, the final design must be thoroughly assessed in a high-fidelity simulation and through linear analysis techniques.

Despite this one drawback, the advantages of the dynamic inversion approach make it very appealing. In addition, the desired dynamics could potentially be made a function of time as well, for example, to make the missile more responsive as it approaches intercept at short time-to-go. The implications of a time-varying design on flight control system performance and on missile performance as a whole are as yet unexplored.

CONCLUSION

This article has covered a variety of topics related to the missile flight control system. The design of this important missile subsystem will continue to evolve to realize the maximum capability of the missile airframe to engage the stressing threats expected in the future.

ACKNOWLEDGMENTS: G. A. Harrison and A. P. Iwaskiw of the APL Guidance, Navigation, and Control Group provided several helpful inputs for this article.

REFERENCES

[1]Jackson, P. B., "A Gradient Projection Algorithm for Missile Autopilot Stability Analysis," in *Proc. AIAA Guidance, Navigation, and Control Conf.* (1992).

[2]Harvey, C., and Stein, G., "Quadratic Weights for Asymptotic Regulator Properties," *IEEE Trans. Autom. Control* **AC-23**(3), 378–387 (June 1978).

[3]Glover, K., and Doyle, J., "State-Space Formulae for All Stabilizing Controllers that Satisfy and H-Infinity Norm Bound and Relations to Risk Sensitivity," *Systems Control Lett.* **11**, 167–172 (1988).

[4]Reichert, R. T., "Application of H-Infinity Control to Missile Autopilot Designs," in *Proc. AIAA Guidance, Navigation, and Control Conf.* (1989).

[5]Ruth, M. J., "A Classical Perspective on Application of H-Infinity Control Theory to a Flexible Missile Airframe," in *Proc. AIAA Guidance, Navigation, and Control Conf.* (1989).

[6]Jackson, P. B., "Applying μ-Synthesis to Missile Autopilot Design," in *Proc. 29th IEEE Conf. on Decision and Control*, pp. 2993–2998 (1990).

[7]Reichert, R. T., "Robust Autopilot Design Using μ-Synthesis," in *Proc. American Control Conf.*, pp. 2368–2373 (1990).

[8]Reichert, R. T., "Dynamic Scheduling of Modern-Robust-Control Autopilot Designs for Missiles," *IEEE Control Systems Magazine* **12**(5), 35–42 (1992).

[9]Nichols, R. A., Reichert, R. T., and Rugh, W. J., "Gain Scheduling for H-Infinity Controllers: A Flight Control Example," *IEEE Trans. Control Sys. Technol.* **1**(2), 69–79 (1993).

[10] Iglesias, P. A., and Urban, T. J., "Loop Shaping Design of a Missile Autopilot—Controller Configurations and Weighting Filter Selection," in *Proc. AIAA Guidance, Navigation, and Control Conf.* (1999).

The Author

Paul B. Jackson is a member of APL's Principal Professional Staff and the supervisor of the Aerodynamic Vehicles Section of the Guidance, Navigation, and Control Group in the Air and Missile Defense Department. He graduated from Washington University in St. Louis in 1988 with a B.S. degree in systems science and engineering and received an M.S. degree in electrical engineering from The Johns Hopkins University in 1992. Since joining APL in 1988 as an engineer in the Guidance, Navigation, and Control Group, Mr. Jackson has worked on many aspects of missile guidance and control, including autopilot design, guidance laws, guidance filtering, seeker control, hardware modeling, and simulation development. These activities have spanned a wide variety of programs including Standard Missile-2 Block IIIB, Block IV, and Block IVA; Tomahawk; and Standard Missile-6. His e-mail address is paul.jackson@jhuapl.edu.

Paul B. Jackson